Structural and chemical evolution in layered oxide battery cathodes revealed by synchrotron techniques

Guannan Qian[1,2], Junyang Wang[1,3], Hong Li[3], Zi-Feng Ma[2], Piero Pianetta[1], Linsen Li[2,4,*], Xiqian Yu[3,*], Yijin Liu[1,*]

[1]Stanford Synchrotron Radiation Lightsource, SLAC National Accelerator Laboratory, Menlo Park, CA 94025, USA

[2]Department of Chemical Engineering, Shanghai Electrochemical Energy Device Research Center (SEED), Shanghai Jiao Tong University, Shanghai, 200240, China

[3]Beijing Advanced Innovation Center for Materials Genome Engineering, Key Laboratory for Renewable Energy, Beijing Key Laboratory for New Energy Materials and Devices, Institute of Physics, Chinese Academy of Sciences, Beijing 100190, China

[4]Shanghai Jiao Tong University Sichuan Research Institute, Chengdu 610213, China

[*]linsenli@sjtu.edu.cn; xyu@iphy.ac.cn; liuyijin@slac.stanford.edu

Abstract

Rechargeable battery technologies have revolutionized the electronics, transportation, and grid energy storage. While many materials are being researched for battery applications, layered transition metal oxides (LTMO) are the dominating cathode candidate with remarkable electrochemical performance. Yet, daunting challenges persist in the quest for further battery developments targeting lower cost, longer lifespan, improved energy density, and enhanced safety. This is in part due to the intrinsic complexity in real-world batteries, featuring sophisticated interplay among microstructural, compositional, and chemical heterogeneities, which motivates tremendous research efforts using state-of-the-art analytical techniques. In this research field, synchrotron techniques stand out as one of the most effective methods for advanced battery characterization in a nondestructive manner with sensitivities to the lattice, electronic, and morphological structures. This article provides a holistic overview of the cutting-edge developments in synchrotron-based research on LTMO battery cathode materials. We discuss the complexity and evolution of LTMO's material properties upon battery operation and review recent synchrotron-based research works that address the frontier challenges and provide novel insights in this field. Finally, we formulate a perspective on the future directions of synchrotron-based battery research, involving the next-generation X-ray facilities and advanced computational developments.

Keywords: layered battery cathode, synchrotron, electro-chemo-mechanical interplay, surface, bulk

Table of Contents

1. Introduction

1.1 Layered transition metal oxide battery cathode.

With a broad range of applications in electric vehicle (EV), grid storage, and consumer electronic, lithium-ion battery (LIB) has become a major player in the global energy storage solution in recent years [1-3]. It is predicted that, in 2025, the global lithium-ion battery market will rise to nearly $100 billion and the shipment volume will reach nearly 440 GWh [4]. The rapid growth of the LIB's portfolio benefits from its favorable characteristics including high energy density, high power density, and environmental friendliness, which also set the targets for further research efforts in this field. While all the battery components are important to the ultimate performance and are subjected to intense research, the LIB cathode remains the most significant bottleneck for further improving the energy density. Among all the materials that are considered and researched as candidates for battery cathode, layered transition metal oxides (LTMO) [5, 6] are the most auspicious. Examples of successfully commercialized LTMO battery cathode include lithium cobalt oxide (LCO) [7-9] for powering consumer electronics and lithium nickel cobalt manganese oxide (NMC) [10-12] in EV applications, demonstrating a tremendous market value.

The LTMO features a layered lattice structure that is essential to the reversible lithium (de)intercalation. As illustrated in Fig. 1a, LTMO exhibits an α-$NaFeO_2$ structure with *R-3m* space group, in which lithium ions and transition metal cations respectively occupy octahedral 3a and 3b sites, while oxygen anions occupy the octahedral 6c sites with cubic close packing [13]. In the layered LTMO lattice, the diffusion of lithium ion strongly favors an in-plane, two-dimensional geometry and is mediated by a divacancy mechanism, in which lithium ion hops to a vacant site that is part of divacancies through a tetrahedral site [14, 15]. Upon battery charging, the extraction of lithium ions from the host LTMO matrix is accompanied by the redox reactions of transition metal cations and, potentially, oxygen anions. The LTMO's lattice structural stability is closely associated with these intertwined redox centers [11, 16]. We show, in Fig. 1b, the electronic structure of four representative elements in LTMO compounds: nickel, cobalt, manganese, and oxygen. The overlap of the Co^{3+}/Co^{4+} t_{2g} band with the top of the O_2 2p band indicates that the empty states undergo a strong anion-p/M-d covalent admixture. For example, the O_2 2p molecular orbitals tend to trap itinerant holes when the LCO was charged above 4.5 V, leading to the O3 → H1-3 phase transitions [17]. The Ni^{3+}/Ni^{4+} e_g band has a smaller overlap with the O_2 2p band. As a consequence, the Ni^{4+} state can be partially reached by extracting more lithium ions without severely jeopardizing the lattice structural stability. Unlike Ni and Co, the Mn^{3+}/Mn^{4+} e_g band has no overlap with the O_2 2p band, resulting in a superior structural robustness. The chemical evolution of oxygen anions in LTMO can have a more profound impact beyond deteriorating the LTMO's structural stability through oxygen release and the associated multiscale structural degradation. Recently, the oxygen redox mechanism in LTMO has drawn a lot of attention (see illustration in Fig. 1c) because, if it is made controllable and reversible, the oxygen redox could be very desirable to the quest for higher capacity and power [18, 19]. In LTMO with multiple co-existing transition metal cations, the interplay among all the different redox centers could distort their respective electronic structures in a complex, interdependent, and dynamic manner, formulating a highly sophisticated electrochemical reaction upon battery cycling.

The strong desire for further advancing the energy/power density and the stability/safety has motivated the development of several new types of LTMO [6, 20], featuring an even higher degree of hierarchical and high-dimensional complexity in structure, morphology, composition, and local chemistry. For example, compositional gradient [21, 22] and ordered primary particle packing [23,

24] are found to be effective for improving the cycling stability. The lattice defect engineering and grain boundary modification, on the other hand, could improve the energy density by promoting the stability at deeply charged states [25-27]. Engineering of the particles formations, e.g., single-crystallization [28-30], is another active research direction that could have a practical impact. To truly unleash the potential of these new LTMO materials, rational microstructure design at the electrode level is indispensable. In Fig. 1d, we illustrate the multi-scale morphological complexity in a real life LTMO cathode from the cell level down to the atomic scale. A practical LTMO composite cathode accentuates distinct surface and bulk reactions that are fundamental to the battery performance. An in-depth and comprehensive understanding of these depth-dependent structural and chemical interplay in LTMO can critically inform the research efforts in this filed. It not only exhibits a tremendous scientific significance, but also is closely relevant to the battery industry. With the enormous amount of effort being devoted into this research direction, here we present a high-level overview of this field with an emphasis on the valuable insights offered by advanced synchrotron characterization techniques.

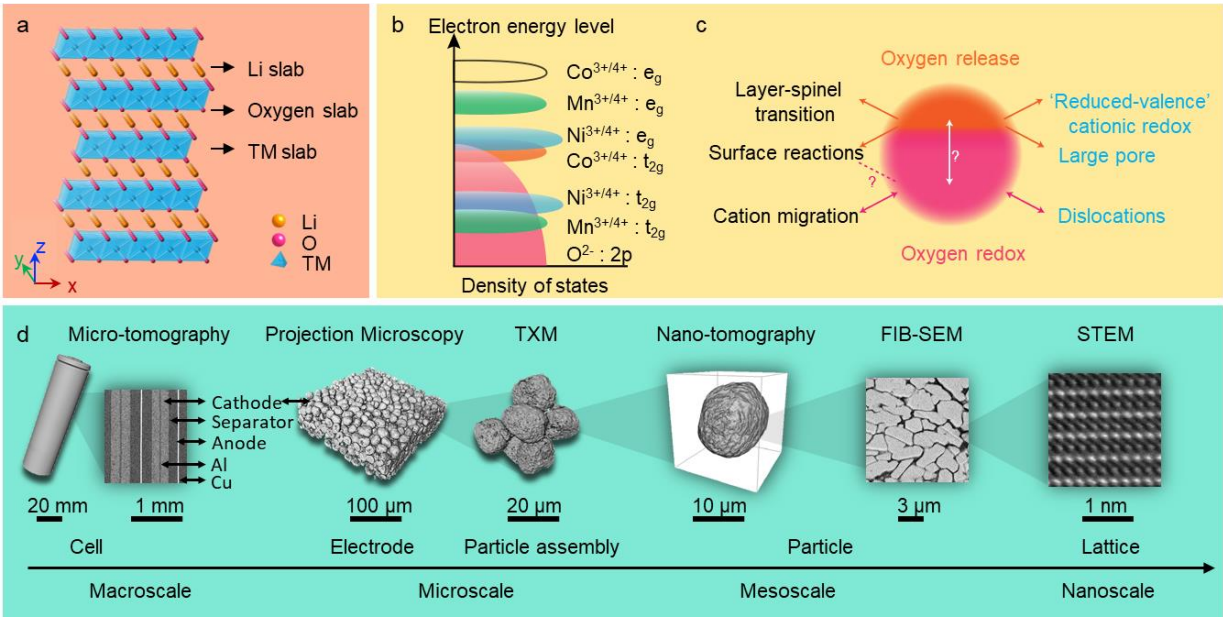

Figure 1. Overview of the lattice structure, electronic structure, and micro morphology of LTMO cathode. (a) Crystal model of layered LTMO (TM: 3d transition metal cations, Ni, Co, or Mn), (b) Schematic illustration of the electronic structures of the key elements in LTMO, (c) Schematic illustration of the oxygen evolution and the associated degradation mechanisms to the LTMO cathode. Adapted with permission from [31] , Copyright 2018, Springer Nature. (d) Multi-scale and high dimensional characterization for real-world LTMO-based LIB.

1.2 Synchrotron characterization techniques.

A systematic investigation of the fundamental yet complicated reaction mechanisms in LTMO relies on advanced characterization techniques. In this respect, synchrotron X-ray techniques have demonstrated unique advantages with excellent multi-scale resolution and multi-modal sensitivity. The principle of synchrotron radiation is based on classical electrodynamics: when a charged particle traveling at a speed close to the speed of light is forced to change its moving direction, electromagnetic radiation will be emitted [32]. Historically, synchrotron radiation was considered as an undesired effect by the particle physicists in the 1950s because it causes the particles to loss

energy [33]. But later on, in the 1960s, scientists began to recognize the synchrotron X-rays as an exceptional tool for a broad range of applications [33]. The tremendous success of synchrotron is evidenced by the exponentially growing research community associated with it, which, in turn, drives the development of several generations of X-ray facilities across the globe [34].

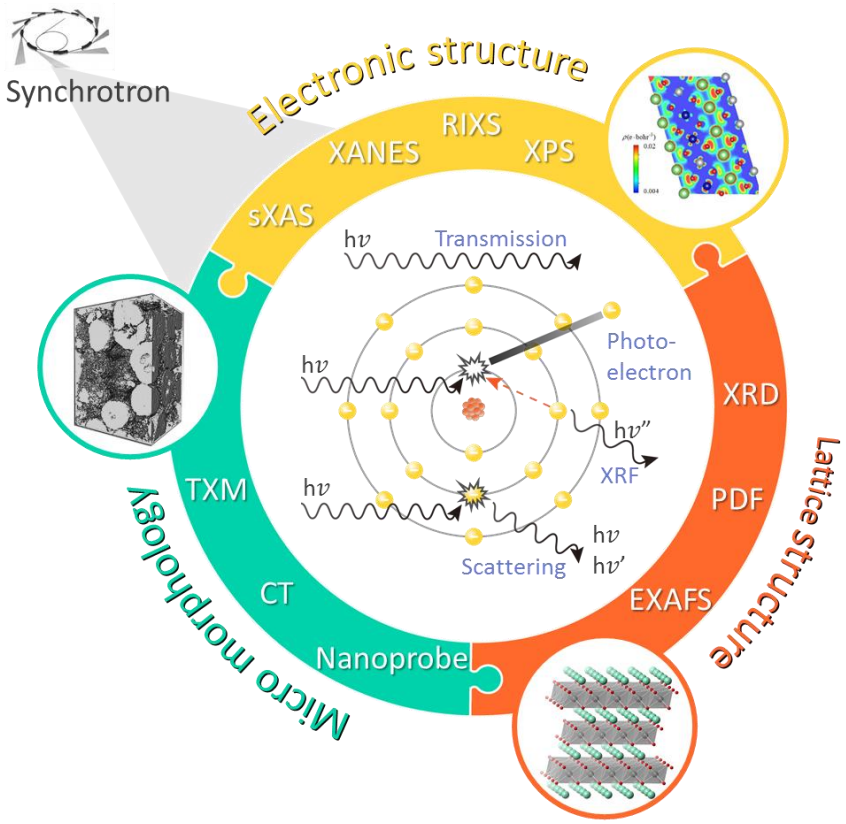

Figure 2. Schematic illustration of the interaction between the synchrotron X-rays and the mater. A number of synchrotron characterization techniques are listed, highlighting their respective sensitivity to the lattice structure, the electronic structure, and the micro morphology.

When X-rays are delivered to the sample, they interact with the matter in a few different ways at different likelihood, leading to several signals that are associated with different material properties, respectively. Generally speaking, absorption, phase-shifting, and scattering are three different basic interactions between the X-rays and the matter, and are most relevant to the X-ray characterization techniques (see illustration in Fig. 2). Absorption refers to the sample's ability to attenuate the incident beam, which is modulated by the X-ray energy level as well as the matter's density and electronic structures, formulating a suite of powerful X-ray absorption spectroscopic (XAS) techniques [35-37]. When an atom absorbs a photon, an electron, e.g., a photoelectron, is kicked out of its orbit, leaving the atom at an exited state. This process can be utilized to conduct X-ray photoemission spectroscopy (XPS), which is sensitive to the elemental composition, the chemical state, the electronic structure, and density of the electronic states over the sample surface [38-40]. The atom's excited state is often unstable and the system will spontaneously

reduce its energy by emitting fluorescence photons or Auger electrons, which facilitate the X-ray fluorescence (XRF) analysis [37, 41]. Scattering is a phenomenon, in which the incident photons are diffused by the matter, changing their direction and propagation. When there is no energy exchange between the photons and the matter, the scattering is elastic and fingerprints the material's lattice structural properties [42, 43]. In the case of inelastic scattering (Compton scattering) [44, 45], the amount of exchanged energy often resonant with and excites the matter. By tuning the incident energy to a targeted absorption edge, it maximizes the cross section for inelastic scattering, opening up the opportunity for detailed electronic structural investigation using resonant inelastic X-ray scattering (RIXS) technique [46-48]. These synchrotron experimental techniques have different penetration depths. Collectively, they can probe the lattice structure, electronic structure, chemical valance state, and multi-scale morphology with high efficiency and precision, which are very relevant to the study of battery materials. More specifically, the change in the battery material's crystalline structure can be monitored using X-ray diffraction (XRD), pair distribution function (PDF), and extended X-ray absorption fine structure (EXAFS) [32]. The states of the chemical and electrochemical redox reactions can be probe by evaluating the elements' chemical valance states with X-ray absorption spectroscopy (XAS, including soft X-ray Absorption Spectroscopy (sXAS) and X-ray absorption near edge structure (XANES)), X-ray emission spectroscopy (XES), X-ray photoelectron spectroscopy (XPS), etc. [49] Advanced synchrotron microscopy techniques can further add 2D or 3D spatial resolution in different experimental configurations, including transmission X-ray microscopy (TXM), scanning micro-/nano-probes, ptychography, and tomography [50]. More recently, several of these techniques are integrated to conduct correlative multi-modal characterization that formulates a more holistic view of the structural and chemical complexity in the LTMO battery cathode under *ex-situ*/*in-situ*/*operando* conditions [51-54]. Another key development in this research field is the implementation of the advanced computational approaches. Impressive achievements and immense potential have been demonstrated using machine learning and data mining algorithms [55-57]. The novel data-driven developments critically complement the synchrotron experimental capabilities by offering the capability to extract the scientifically important information from the large-scale experimental data effectively and efficiently with greatly reduced human labor and error.

In this article, the application of synchrotron techniques in studying LTMO battery cathode materials will be reviewed from three different perspectives: the lattice structures, electron structures, and multi-scale morphology, as illustrated in Figs. 1 and 2. We will systematically discuss the relevant techniques and the scientific implications will be summarized with a focused theme on the depth-dependent structural and chemical interplay and evolution in LTMO upon battery cycling. Finally, we will conclude our review by discussing the future perspectives, including the data science approaches, the projected major synchrotron and X-ray free electron laser upgrades, and their impact on the research for next-generation high energy and power density battery materials.

2. Synchrotron characterization of LTMO's lattice structural complexity and evolution

2.1 Complexity and evolution in LTMO's lattice structure.

The traditional lithium-stoichiometric $LiTMO_2$ (TM=Ni, Co, Mn, etc.) have a cubic close-packed oxygen framework with an AB-CA-BC stacking sequence (O3-type structure in the notation of

Delmas [58]), exhibiting a rhombohedral α-$NaFeO_2$ type structure with *R-3m* space group (Fig. 3a). In the structure, transition metal cations locate at octahedral 3b sites between oxygen layers, forming TM slabs consisting of edge-sharing TMO_6 octahedra, whilst lithium ions occupy the octahedral 3a sites in Li slabs, which can reversibly extract/insert from/to the Li sites between the TM slabs. Typical lithium-stoichiometric LTMO cathodes sharing the O3-type structure include $LiCoO_2$, $LiNiO_2$, and their derivatives, such as $Li(Ni_xCo_yMn_{1-x-y})O_2$ (NMC), and $Li(Ni_xCo_yAl_{1-x-y})O_2$ (NCA). Lithium-rich LTMOs ($Li_{1+x}TM_{1-x}O_2$), derived from the parent lamellar $LiTMO_2$, are created by partially substituting transition metal cations with excess lithium ions on the TM slabs. As a result, it leads to the formation of a Li-TM_6 honeycomb-type superstructure, which lowers the symmetry of material structure from *R-3m* to monoclinic *C2/m* symmetry. For example, Li_2MnO_3, alternatively noted as $Li[Li_{1/3}Mn_{2/3}]O_2$, exhibits an O3-type layered structure with *C2/m* symmetry, which has one-third of Mn^{4+} in TM slab replaced by Li^+ ions to form honeycomb Li-Mn_6 superstructures (Fig. 3b). The superlattice ordering on the TM slabs results in the peculiar Bragg peaks in the range of ~ 20° to 35° (*Cu* K_α). This in-plane ordering of Mn^{4+}/Li^+ cations also appears in other lithium-rich manganese-based LTMOs and forms local superlattice structure [59].

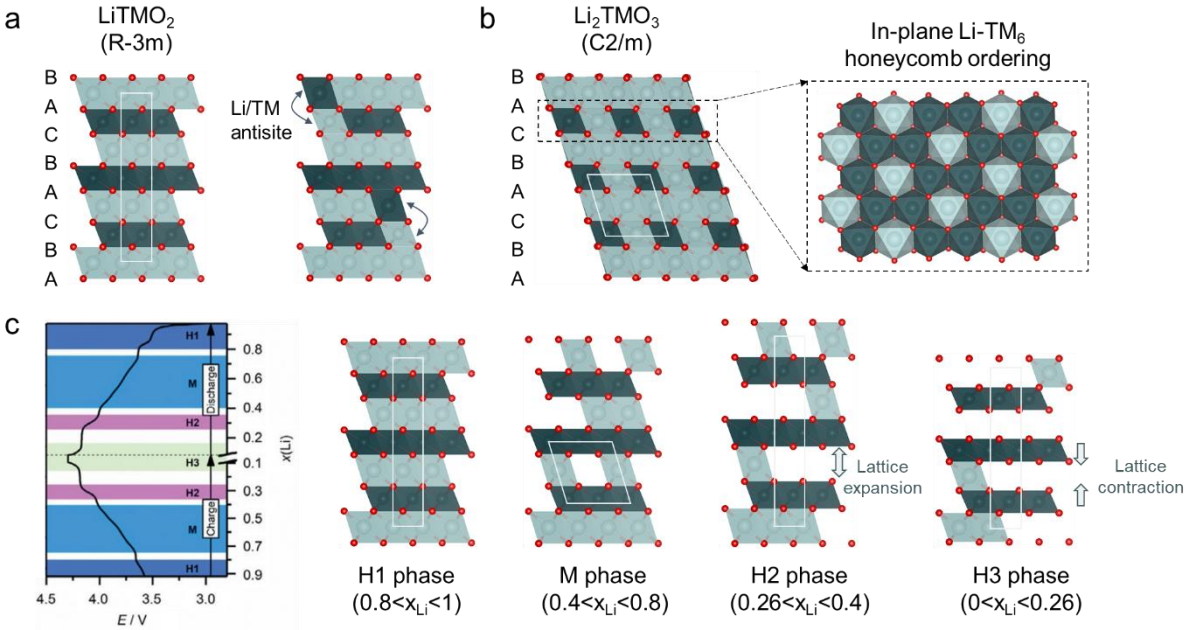

Figure 3. Illustrations of crystal structures relevant to the layered LTMO cathodes. (a) O3-type stacking sequence and cation antisite defects of $LiTMO_2$ in the hexagonal lattice. (b) Monoclinic unit cell of lithium-rich LTMO cathode Li_2TMO_3 with an in-plane Li-TM_6 honeycomb-ordering. (c) Lattice structure evolution of layered $LiTMO_2$ cathodes during the first deintercalation process. Adapted with permission from [60], Copyright 2020, Wiley-VCH.

Other than the ideal scenario, where TM ions and Li-ions always occupy their specific sites in the LTMO's lattice, crystalline defects also can be feasibly generated in the lattice structure, which significantly increase the structural complexity of LTMO. Noteworthily, those structural defects can play a key role in determining the electrochemical properties of LTMOs. For example, Li/Ni antisite defects, also referred to as "Li/Ni mixing", are commonly observed in Ni-rich LTMOs such as $LiNi_{0.8}Mn_{0.1}Co_{0.1}O_2$ (NMC811). The Ni^{2+} ions sitting in the Li site of Li slabs can affect

the Li^+ diffusion kinetics in the lattice structure and even cause structural collapse during the charging process as Ni^{2+} is oxidized to smaller sized Ni^{3+}, which blocks the Li^+ mobility. Though the Li/Ni antisite defects in LTMO are generally attributed to the similar size of Li^+ (0.076 nm) and Ni^{2+} (0.069 nm) in most of the previous research works [61], it cannot explain the finding of increased amount of Li/Ni antisite defects in the Ni-based LTMOs with more Ni^{3+} (0.056 nm). Hence, Zheng *et al.* have proposed a new mechanism for the formation energy of Li–Ni antisite defects in terms of a super-exchange interaction between TM atoms [62]. It can be mainly affected by two factors: (1) the extent of structural distortion that can be quantified by the change of bond length after occupant's exchange in the Li and TM sites and (2) the difference of super-exchange interaction between various configurations of TM^{x+}-O^{2-}-TM'^{y+}, which changes with the formation of the antisite defects.

The antisite defects in the material structure can be generated not only during the material synthesis but also during the electrochemical cycling. For example, Shao-horn *et al.* reported the finding of cations migration from the transition-metal slabs to Li slabs during electrochemical cycles by using TEM analysis [63]. Independently, Kang *et al.* reported that the surface structure of $LiNi_{0.5}Co_{0.2}Mn_{0.3}O_2$ undergoes a phase transition from a O3 phase (*R-3m*) to a spinel-like structure (*Fd-3m*) or rocksalt phase (*Fm-3m*) because of the TM cations migration during electrochemical cycling [64]. At a deeply charged state, the layered structure of LTMO materials becomes extremely unstable due to the increased structural stress caused by the empty lithium sites. Thus, it prompts TM cation migration from TM layer to lithium layer. The TM migration tends to occupy every second Li vacancy to relieve the electrostatic repulsion between the disordered cations and antisite defects are thereby progressively accumulated in the material structure during an extended cycling process.

The TM_{Li}-V_{TM} antisite defects induced by TM migration during charging have been identified experimentally using various analytical tools. It has been found that limited reversibility of intra-cycle TM migration results in the continuous growth of spinel-like disordered phases in the electrode materials, which is commonly associated with the voltage decay of the batteries [65]. Consequently, exacerbated voltage fade is found in Li-rich NMC upon extended cycling as more TM ions were trapped in the Li layer [66]. However, it is important to mention that the fundamental mechanism for the observed voltage decay is not essentially determined by the TM migration behaviors but the resulting confinement of TM ions in the Li layer [67], which suggest that a reversible TM migration behavior between TM layers and Li layers will not necessarily lead to the voltage decay of the batteries. Unfortunately, at a state of low Li stoichiometries for most lithium-rich LTMOs, TM migration to the Li layer is a thermodynamically favored and irreversible phenomenon during the charging process. As such, various approaches such as surface coating, cation doping, adding electrolyte additives, and composition tuning, have been used to mitigate the TM migration. A complete prevention of the voltage decay over long-term cycling, however, remains a daunting challenge.

Besides the antisite defects, lattice stacking disorder is another common structural defect in layered LTMOs, while the TM slabs might have an in-plane cation ordering. Thereby, it significantly increases the lattice structural complexity and the difficulties for structural characterization. First, the occurrence of stacking disorder defects causes diffuse scattering of the lattice structure and leads to a considerable broadening of the superlattice reflections. Second, different stacking sequences of the TM slabs along the *c* axis in LTMOs generate different lattice symmetry for the materials [68]. For example, Breger and Meng *et al.* have proposed two different ways of stacking

in Li_2MnO_3, where A1-B1-C1 corresponding to *C2/m* and A1-B1-C2 corresponding to *P3₁12* space groups [69]. Using these space groups, XRD patterns of Li_2MnO_3 can be well simulated and the *C2/m* stacking scheme is found to be better in evaluating the stacking fault probabilities.

Moreover, Meng *et al.* also pointed out that the generation of the *P3₁12* lattice symmetry can be attributed to an abnormality of the *C2/m* sequence [70]. In parallel, Riou *et al.* have proposed an A1-B1-C2-A2-B3-C1 stacking sequence to explain the lattice structure of Li_2MnO_3 with a symmetry of the *C2/c* space group [71]. Such an inconsistency in their interpretation can be caused by the negligible energy difference between the proposed lattice sequence of the lattice structure, which is very sensitive to the synthesis temperature and thereby lead to random stacking faults in Li-rich LTMOs. Moreover, upon lithium removal from the lattice of LTMOs during charging, oxygen slabs tend to glide toward each other, and a structural rearrangement happens in the materials. As a consequence, a distorted ccp oxygen lattice (at different degrees) and a hexagonal close packing of oxygen can form in the lattice structure if a large portion of Li ions are removed. Therefore, a series of irreversible phase transitions are frequently observed in the $LiTMO_2$ upon a deep extraction of Li-ion.

Specifically, pristine $LiTMO_2$ first undergoes a solid-solution reaction until the state of charge at ~$Li_{0.8}TMO_2$. It then proceeds a phase transformation from a hexagonal symmetry (H1 phase) to a monoclinic symmetry (M phase). This monoclinic phase of distorted O3 structure has a decreased lattice symmetry for *C2/m* compared to *R-3m*. The monoclinic phase can often be observed in layered cathodes because of lithium/vacancy ordering and/or collective Jahn-Teller (JT) distortion caused by the active cations such as Ni^{3+}. While the lowering in symmetry from hexagonal to monoclinic generally occurs in a range of $x \approx 0.8$-0.4 for the Li_xTMO_2 compositions. It further evolves into the M phase (H2) between $x \approx 0.40$ and 0.36, and the H2 phase remains until $x \approx 0.26$. Further, for the range of $x \approx 0.26$-0.16, order H2-H3 phase transition occurs, which is usually found at ~4.2 V versus Li. Thus, the H3 phase, which has a substantially smaller *c* parameter compared to the H2 (Fig. 3c) [60], forms through a biphasic process despite the energetically costly and highly strained H3/H2 interface. It raises the question on the origin of the thermodynamic driving force for the phase separation. A similar two-phase reaction, associated with a drastic decrease in the interlayer distance, is the phase transformation from O3 to H1-3 observed in Li_xCoO_2 upon charging to ~4.6 V versus Li, which further transforms into an O1 structure with a higher extend of delithiation at a higher voltage range. Meanwhile, the H1-3 phase has never been reported for Ni-rich LTMOs, which implies that the H3 phase is unlikely to be an H1-3 structure. Instead, a phase transition from H3 to O1 has been observed for Ni-rich LTMOs when charged to 4.2 V or 4.45 V, which suggests that the onset voltage for the occurrence of such phase transition should be lower than 4.2 V versus Li.

Importantly, the kinetics of this phase change can be very sluggish, as it is observed under a condition of extremely slow charging for the LNO samples with low amounts of antisite defects [72-74]. This observation is likely to be caused by the presence of Ni in the Li layer that hinders the complete delithiation process and therefore impede a change in the stacking sequence. Indeed, for Ni-rich LTMOs with antisite defects at a concentration greater than 7%, the H3 → O1 transition can no longer be observed [75]. Therefore, it is hypothesized that the presence of an appropriate amount of antisite defects in the material structure could be beneficial for Ni-rich LTMOs, as it can suppress the H3 → O1 transition.

2.2 Synchrotron-based structure characterization techniques and their applications.

The lattice structures of cathode materials are closely related to the battery performance metrics, e.g. power and energy density, cyclic life, and safety performance [76]. Thus, an in-depth understanding of the relationship between the material structure and the performance is pivotal to the optimization of the current cathode material systems as well as to developing new cathode materials with superior electrochemical properties. Therefore, it necessitates the study of structural evolution that occur in the cathode materials during the electrochemical processes, which could include changes in the lattice parameters, phase transition, and atomic occupancy.

In-situ XRD is a widely used method for probing the crystal structure and phase transformation for crystalline electrode materials during cycling. For instance, Zhou *et al.* have utilized *in-situ* XRD to investigate the structural evolution of Li_2MoO_3 cathode during the charge-discharge process and found an "abnormal" unit cell breathing mechanism for the cathode materials [77]. As shown in Fig. 4a, all the peaks in the XRD patterns of pristine and charged Li_2MoO_3 can be indexed to a layered structure with the *R*-3*m* space group. The *in-situ* XRD patterns of the $Li_{2-x}MoO_3$ electrode during charging demonstrated a solid solution reaction that occurs in a region of $0<x<0.5$. All the main X-ray reflections in the patterns are found to shift toward the lower angle side, indicating an increase in the *d*-spacing of phase I. Subsequently, a new phase (phase II), which shares the similar layered structure with phase I but with larger lattice parameters, emerges in the region of $0.5<x<1$, suggesting the occurrence of a two-phase reaction. With the delithiation further proceeds over $x>1$, phase I disappeared, and a solid solution reaction of phase II was observed. Interestingly, while the widely used layered $LiMO_2$ (M = Co, Ni, Mn) shows shrinkage in the lattice parameters of *a* and *b* during charging, the Li_2MoO_3 exhibits a reversed trend of the lattice parameter's evolution. Such "abnormal" behavior can be explained by the specific attributes of the metal-metal bonding in the materials that control the *a(b)* evolution during charging.

When comes to the design of battery materials for high power applications, it is crucial to have a fundamental understanding of the structure evolution that occurs in the electrode materials during the fast charge – discharge process, which could be quite different from that of the electrode materials charged at a low current rate. Thus, time-resolved X-ray diffraction (TR-XRD) techniques have been developed to investigate the fast dynamic properties of electrode materials that charge at high current rates. Taking advantage of the fast data acquisition capability and high brightness of synchrotron X-ray beams, Zhou *et al.* have conducted time-resolved *in-situ* synchrotron XRD to investigate the charge-rate dependent phase transition process of layered $LiNi_{1/3}Mn_{1/3}Co_{1/3}O_2$ [78]. As shown in Fig. 4c, both the charging processes of the material under the current rates of 0.1 and 1 C show two regions of solid solution reactions of hexagonal phases of H1 and H2, along with a two-phase coexistence region of H1 + H2 in between. Importantly, with the charging rate further increases to 10 C, a new intermediate phase was observed in between the two solid solution reaction regions, while the peaks of this structure become increasingly pronounced at even higher rates of 30 C and 60 C. Besides, an abnormal Li-poor region with tetrahedral Li occupation and a normal Li-rich region with octahedral Li occupation were observed in the partially charged sample using scanning transmission electron microscopy (STEM). Thus, it suggests that the intermediate phase can act as a buffer between the Li-rich and Li-poor phases, which could reduce the local stress and strain produced by inhomogeneity during charging and, therefore, stabilize the material structure.

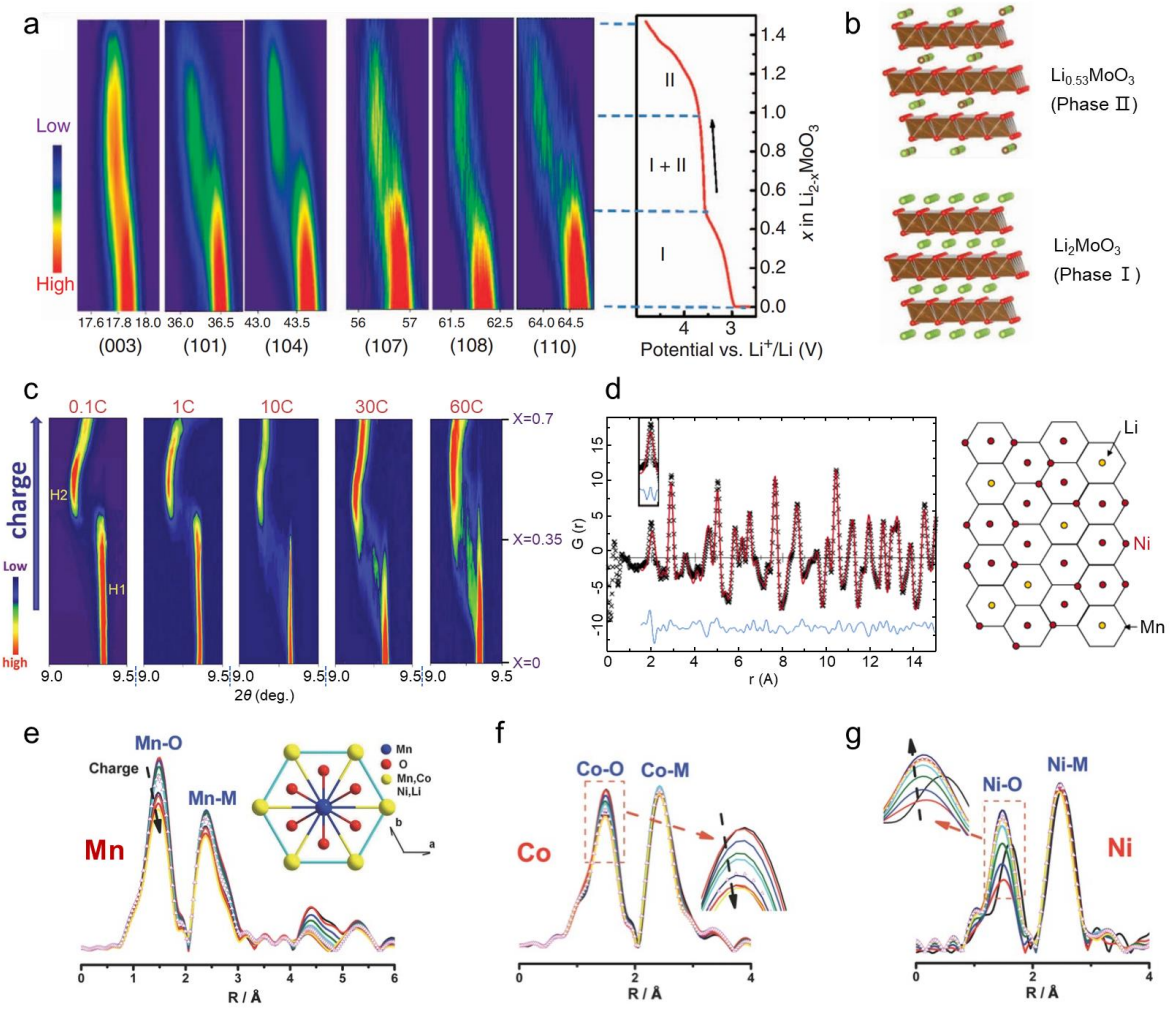

Figure 4. Synchrotron-based structural studies of LTMO cathode materials. (a) *In-situ* XRD pattern and charge curve of $Li_{2-x}MoO_3$ cathode during delithiation. Adapted with permission from [73], Copyright 2014, Springer Nature. (b) Structure models for two phases formed during the charge process. Adapted with permission from [77], Copyright 2014, Springer Nature. (c) *In-situ* XRD of $LiNi_{1/3}Mn_{1/3}Co_{1/3}O_2$ during the first charge at different C rates (0.1, 1, 10, 30, and 60 C). Adapted with permission from [78], Copyright 2016, WILEY‐VCH. (d) Pair distribution function $G(r)$ of $LiNi_{0.5}Mn_{0.5}O_2$ obtained from synchrotron X-ray total scattering and the in-plane cation ordering of $LiNi_{0.5}Mn_{0.5}O_2$ derived from RMC refinement. Adapted with permission from [79], Copyright 2005, American Chemical Society. (e-g) Fourier transformed EXAFS Mn, Co, and Ni K-edge spectra of $Li_{1.2}Ni_{0.15}Co_{0.1}Mn_{0.55}O_2$ collected during the initial charge process. Adapted with permission from [80], Copyright 2013, WILEY‐VCH.

Although XRD techniques are very useful for the structural analysis of crystalline materials, it provides limited structural information for the sample without long-range order, such as amorphous materials and materials in the form of nano-sized crystals. For example, it is hard to probe the reaction mechanism of a conversion-type electrode material using XRD due to the nature of nano-sized and highly disordered particles formed during the conversion reaction process. To

resolve this issue, the pair distribution function (PDF) have been utilized for battery research, complementing the XRD approaches. While XRD only concerns Bragg scattering and provides long-range average structural information, the PDF technique can investigate the local structure of the materials with short-range ordering by utilizing the total scattering signal, including both Bragg and diffuse scatterings [81]. Specifically, it can provide local information regarding the atomic pair distribution, which relates to chemical, structural, and morphological transformations that occur during the electrochemical reactions.

A typical example to explain how PDF reveals the short-range ordering in $LiNi_{0.5}Mn_{0.5}O_2$ material is provided by Breger *et al.* (Fig. 4d). They reported that strong site occupation correlation exists between Ni and Mn cations in the first and the second coordination shells, which leads to non-random distribution in a short-range scale [79]. A reverse Monte-Carlo (RMC) simulation of the PDF data has been conducted using a "big box" structure model for the material, which contains hundreds to thousands of atoms. Through this approach, several hidden structural features of short-range ordering in the material are revealed. One is that the Ni cations tend to be surrounded by Mn cations in the first coordination shell and be surrounded by Li and Ni cations in the second shell. Another structural feature is that about 10% of Li/Ni mixing exists in the structure, meaning about 10% of Li ions from the Li layer exchange with Ni cations in the TM layers. Moreover, the Li ions in the transition metal layer are likely to prevent Ni cations in their first coordination shell but tend to be surrounded by Mn cations. These local structural features cannot be deduced from fitting the conventional XRD patterns, which are associated with the average bulk structure of the material. Therefore, combining PDF data with advanced fitting/simulation methods can be an effective method to unlock the hidden structural information for various battery materials.

In addition to the PDF, X-ray absorption fine structure spectra (XAFS) is also a powerful technique for studying the local structure around active atoms at atomic and molecular scales. Based on the energy range, an XAFS spectrum can be divided into two regions, XANES and EXAFS. While the XANES spectra can provide information regarding the electronic structure and local chemical environment, the EXAFS spectra are primarily used to determine the local structural information, including bonding distances, coordination number, neighboring atom species, lattice distortion, and phase transformation. Since these local lattice structure plays important roles in modulating the ionic diffusion, phase composition, and electrochemical reaction mechanisms, probing the local structural properties is crucial to constructing a full-view of the material structure and to enabling a rational material design for improved electrochemical performance.

EXAFS analysis has also been applied to track the change of crystal structures and structural instability of LTMO cathode over cycling, which is closely related to the capacity degradation mechanism of LTMO. For example, Kim and Yo *et al.* utilized EXAFS to study the change in interatomic distance and structure distortions in $LiCo_{0.85}Al_{0.15}O_2$ during delithiation [82]. As elucidated by the *k*-space and *R*-space spectra obtained from EXAFS analysis, all bond pairs showed a decrease in interatomic distance and the crystal structure displayed an increase in distortion with the increased Debye-Waller factor. Thus, the change of local structures of the cathode material can be a major reason for the capacity degradation. Separately, Tsai *et al.* conducted *in-situ* XAFS to study the structural evolution in the NMC cathode upon cycling [83]. The *in-situ* XAFS data confirmed that the charge compensation mechanism of the NMC cathode is mainly contributed by Ni and O, as its demonstrated by the change of Ni-O bond length with the Ni^{2+} oxidization. While the structural distortion is revealed by the change of Debye-Waller factor as the Ni^{3+} is the JT effect active species, which can cause a change in the bond length during

the charge and discharge process. Further, Yu *et al.* applied *in-situ* XANES and EXAFS to study the local structure changes around Ni, Mn, and Co in Li-rich layered $Li_{1.2}Ni_{0.15}Mn_{0.55}Co_{0.1}O_2$ during the first charge [80]. Although the edge energy of the Mn and Co K-edge spectra maintains the same position during the delithiation process, the shape of the XANES spectra and the Fourier transformed (FT) EXAFS spectra show obvious changes in the peak intensity of Co-O and Mn-O bonds. This phenomenon suggests that Mn and Co are responsible to the charge compensation process for this electrode material during delithiation, which have a varied tendency for the process in different states of charge (Fig. 4e-g). Based on the EXAFS analysis, Co and Mn are proposed to be mainly related to the voltage slope and voltage plateau regions, respectively. With further analyzing the Debye-Waller factors, changes in the local environment around Mn also suggest the Mn-related structural distortion behavior, which can be an important reason for the capacity fading over prolonged cycling. Thus, *in-situ* EXAFS has been utilized for elucidating the local structure evolution and charge compensation mechanism for the Li-rich layered $Li_{1.2}Ni_{0.15}Co_{0.1}Mn_{0.55}O_2$, which is found to be different from that of the conventional NMC.

Taken together, these studies on the electrochemical behavior of various cathode materials have constructed an in-depth understanding of the electrochemical process for the LIBs, which is of significant value to the design, synthesis, and development of advanced cathode materials in the future.

3. Synchrotron characterization of LTMO's electronic structural complexity and evolution

3.1 Complexity and evolution in LTMO's electronic structure.

The repeated energy storage and release in a "rocking chair" battery features a back-and-forth conversion process between electric energy and chemical energy. The total amount of energy produced/stored by discharging/charging a battery is determined by the change in the Gibbs free energy (ΔG) of the system [84]. ΔG can be measured by the maximum amount of work that can be performed during this energy conversion process, which is described by the classic Nernst Equation: $\Delta G_S = -nFE_S$, where ΔG_S is the change in the standard Gibbs free energy of the system, n is the number of moles of electrons, F is Faraday constant, and E_S is the standard potential of the battery. That is to say, the total amount of charge transferred during the chemical reaction and the corresponding cell potential collectively determine the capacity of the battery. In LTMO-based batteries, these two key parameters are derived from the properties of the transition metal (TM) cations, e.g., Ni, Co, and Mn as well as the redox active anions, e.g., O. Therefore, it is vital to thoroughly characterize the electronic structures of these elements for a better understanding of the cathode properties and, subsequently, for improving the battery performance.

In practical electrochemical systems, the complexity in the redox reactions stems from several co-existing and intertwined redox centers. For example, due to the partial overlap between t_{2g} band of Co and 2p band of O, both Co^{3+} and O^{2-} can be oxidized when more than 0.5 Li are extracted from the LCO lattice, leading to a capacity decay [11]. In pristine $LiNi_{1/3}Co_{1/3}Mn_{1/3}O_2$ (NMC-333) cathode the TMs' initial oxidation states are Ni^{2+}, Co^{3+}, and Mn^{4+}, respectively. The redox activities of Ni^{2+}/Ni^{4+} and Co^{3+}/Co^{4+} dominate the charge compensation below 0.65 delithiation, whereas the oxidation state of Mn^{4+} is mostly unchanged [85]. Oxygen, however, can impact the system throughout the entire potential window through TM-O hybridization. In particular, at a deeply delithiated state (above 0.65 delithiation), the oxygen anions could become redox active. It is also reported that the oxygen redox is related with its local TM species, which is rather

complicated due to the participation of multiple elements [85]. This interplay has also been reported in $Li_{1-x}Ni_{0.88}Co_{0.1}Al_{0.02}O_2$ (NCA) cathode [86]. It is suggested that the Co cation can compensate the charge in parallel with the Ni cation through t_{2g}-e_g hopping. In Li-rich NMC materials, oxygen redox becomes an important contributor to its total capacity. In general, the lattice oxygen release/oxidation [87] or the formation of localized electron holes on the oxygen anions around Mn^{4+} and Li^+ [88] are proposed as possible mechanisms of the oxygen redox process. The respective fractions of capacity contribution from Ni, Co, Mn, and O could dynamically evolve as the cell is repeatedly cycled [18]. This has been identified as one of the root causes for the voltage and capacity decay in Li-rich cathode materials.

To improve the performance of LTMO cathode, a number of different approaches have been carried out. Examples include doping and coating, structural design, and compositional optimization [89]. These approaches have demonstrated significant impacts on the LTMO's electronic structures. As an example of the doping and coating approach, Titanium (Ti) was used to regulate the electronic structure on LCO surface to improve the stability of LCO at high voltage [90]. The unoccupied O 2p states above the Fermi level are largely suppressed on the Ti-rich surface, where the charge deficiency is decreased. The O anions around Ti cations lose less charge compared with those far from the Ti cations, inhibiting the irreversible oxygen redox [90]. The electronic conductivity of LCO can be improved by doping magnesium. By introducing ~5% Mg in LCO, the electronic conductivity is increased to ~0.5 S cm^{-1}. That is because Mg^{2+} partly substitutes Co^{3+}, leading to a decrease of Li vacancies in order to keep the charge neutrality [91]. In term of structural optimization, nanosized LCO has been considered as high-power cathode candidate, which benefits from its anisotropic surface and short Li-ion diffusion length [92]. In addition to nanosizing, the lattice facet engineering is also demonstrated to be effective. The valance state of Co deduced from surface to inner in (003) plane, whereas no apparent changing in the ab-plane [93]. The former can lead to surface effect along c-direction that benefit Li-ion diffusion. Compositional optimization is another popular approach that have shown great potential. In charged NMC cathode, the high valent Ni is active and can oxidized the electrolyte. This side reaction can lead to the loss of active materials as well as the increase of impedance. Sun *et al.* designed a full-gradient NMC material that is Mn-rich on the surface and Ni-rich in the core region [21]. The Mn's 3d band is more inert and the Mn-rich surface can efficiently suppress the interphase side reactions and improve the cathode stability. Lin *et al.* demonstrated that the self-assemble effect in a spray pyrolysis process can also achieve a depth-dependent compositional heterogeneity with similar characteristics [52]. To suppress the voltage decay in Li-rich NMC materials, Sun *et al.* demonstrated a control of the local electronic structure through tailoring the chemical composition [94]. By increasing the Ni content in Li-rich NMC, the oxidation state of TMs, especially for Mn, can be increased. The TM 3d – O 2p band and non-bonding O 2p band shift toward lower energy, leading to an increment in the operating voltage and a suppression of the voltage decay.

In general, the cathode materials' electronic structures are critical to the battery performance because the redox behaviors are directly correlated with the energy density and stability of LTMO and their dynamic evolutions can further complicate the system. Synchrotron X-ray techniques have unique advantages in probing and resolving the electronic structures both in the bulk and on the surface of the LTMO cathode. In the next section, several synchrotron X-ray spectroscopy techniques for elucidating the electronic structures will be reviewed and their applications in studying LTMO materials will be highlighted.

3.2 Synchrotron spectroscopic techniques and their applications in LTMO studies.

Depending on the X-ray energy and the detected signals, several different X-ray spectroscopy techniques have been broadly applied to energy material research. Before going into more detailed discussions, we first clarify that some of these X-ray spectroscopic techniques are not limited to the synchrotron facilities. For example, the tabletop X-ray based XPS, which detects and resolves the energy of photoelectrons, is widely available for characterizing the chemical states over the material surface. The use of a tabletop X-ray source is associated with a relatively low intensity and a very limited energy tunability (e.g., Al Kα radiation of 1.49 keV) [95], which set some practical constrains, e.g., in probing depth (< 5 nm for 1.49 keV) and in chemical sensitivity. When implemented with a synchrotron source, XPS can be carried out at different photon energies, opening up significant scientific opportunities. For example, the probing depths can be effectively adjusted by varying the incident X-ray energy for hard X-ray photoelectron spectroscopy (HAXPES, 13 nm at 3.0 keV, 29 nm at 6.9 keV, and 40 nm at 10 keV) [96]. The chemical state can, therefore, be characterized in a depth-dependent manner through this approach. In the study of materials with very fine particle size (~100 nm or smaller), it can even be considered as a "bulk sensitive" technique. HAXPES has been be utilized to study the chemical state, composition, and their depth-dependent interplay in LTMO cathode materials. Here we discuss a HAXPES study, by Assat *et al.*, on the charge compensation mechanism for the anion redox in Li-rich NMC cathode [97]. As shown in Fig. 5a, the first charged and discharged Li-rich NMC cathodes were tested using HAXPES with different probing depths. The surface deposits' contribution to the O 1s photoelectron signal decreases as the incident photon energy increases from ~1.5 keV to 6.9 keV. The intensity of O^{n-} and its ratio (the percentage of oxidized lattice oxygen) do not change significantly as a function of the depths, suggesting that the O^{n-} exists both on the surface and in the bulk. The charge-compensation mechanism can be speculated based on the evolution of % O^{n-} as a function of the state-of-charge. The authors also reported that the variation of % O^{n-} is rather consistent in the first and second cycles, suggesting a fairly good reversibility of oxygen redox in the early cycles of this material. The incomplete reduction of oxygen when discharged to 2.0 V hints its sluggish kinetics and can be associated with the capacity loss in the first cycle. It is suggested that a potentiostatic hold at 2.0 V may be necessary in the discharging process for reducing O^{n-} toward the full extent.

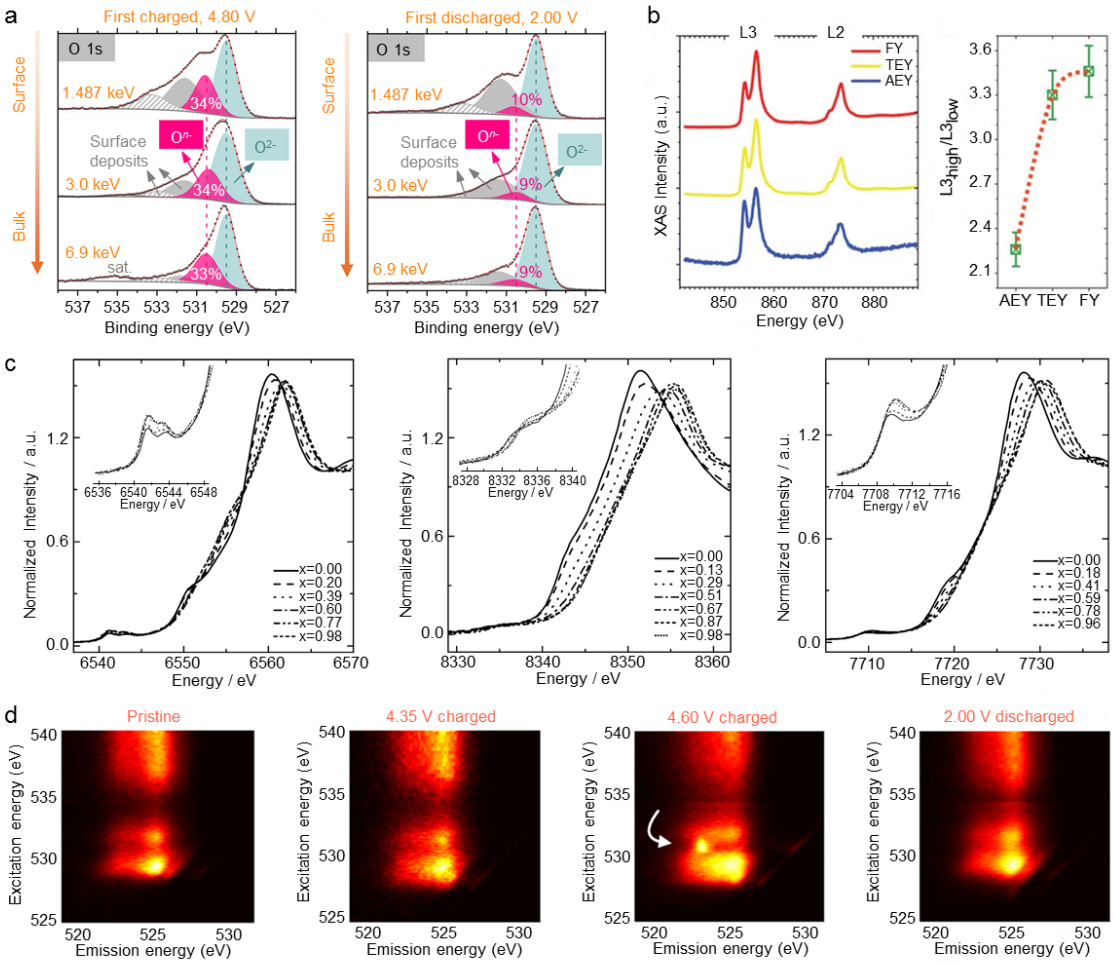

Figure 5. Synchrotron-based X-ray spectroscopic studies of LTMO cathode materials. (a) Depth dependent XPS signal from Li-rich NMC cathode revealed by HAXPES. Adapted with permission from [97], Copyright 2017, Springer Nature. (b) sXAS data on NMC cathode in FY, TEY, AEY modalities. Adapted with permission from [98], Copyright 2014, Royal Society of Chemistry. (c) Hard X-ray XANES data over the K-edges of Ni, Mn, and Co in an NMC cathode. Adapted with permission from [99], Copyright 2005, American Chemical Society. (d) Soft X-ray RIXS data on a Li-rich NMC cathode at different state-of-charge. Adapted with permission from [100], Copyright 2017, Springer Nature.

As we have discussed in the previous section, when an X-ray photon is absorbed by the mater, a core-level electron is excited to the unoccupied states above the vacuum or Fermi level. When the energy of the photon resonates with the ionization potential of a certain quantum state, the absorption cross-section is maximized and the resulting discontinuity in the absorption spectrum that is referred to as an absorption edge. The energy shift of the spectrum often reflects a change in the oxidation state, while the spectrum shape is related with the local chemical environment and the ligand geometry. Therefore, the X-ray absorption spectrum is often used to fingerprint different chemical species. Table 1. lists the absorption edges and their corresponding energy for the primary elements in LTMO material [101]. Here we discuss a few different spectroscopy techniques, including sXAS, XANES, and RIXS, all of which have demonstrated valuable contribution to the understanding of the electronic structures in LTMO materials.

Most of the sXAS beamlines can cover the transition metal *L*-edges and O *K*-edge and can probe the valance band of TM 3d and O 2p states. In a sXAS scan, different signals can be detected, formulating different operation modes include Auger electron yield (AEY), total electron yield (TEY), and fluorescence yield (FY). The probing depth of these signals varies, featuring different depth sensitivities: 1-2 nm for AEY, 2-5 nm for TEY, and 50 nm for FY [98]. In most case, these signals can be detected concurrently for a depth dependent electronic structural analysis. To study the electronic structures of nickel in NMC materials, Lin *et al.* performed Ni *L*-edge XAS at different SOC of the first cycle (Fig. 5b) [98]. The Ni L_3-edge splits into high-energy ($L_{3\text{-high}}$) and low-energy ($L_{3\text{-low}}$) peaks due to the Ni 2p – Ni 3d electrostatic interaction and the crystal field effects. The ratio between $L_{3\text{-high}}$ and $L_{3\text{-low}}$ is positively correlation with the nickel's oxidation state. By comparing the AEY, TEY, and FY signals, a depth-dependent variation in nickel's oxidation state was observed in the charged electrode (Fig. 5b). The reduced Ni cation on the surface of NMC cathode is often attributed to the surface reconstruction effect, which refers to the transformation of layered structure into spinel/rock salt structures due to undesired side reactions on the cathode surface. A follow-up study by the same group highlights that the liquid electrolyte plays a significant role in the surface reconstruction process and the Ni is more prone to reduction at higher state-of-charge [53]. The application of this depth-dependent sXAS approach was further extended to studying the thermal stability of LTMO, which is relevant to the lattice structure degradation, oxygen release, and exothermic side reactions that could provoke a battery thermal runaway. In this respect, sXAS can reveal the thermal decomposition paths and the related degradation mechanisms. Alvarado *et al.* showed the evidence of reduction of Co and Ni in delithiated NMC-811 after heating using Co and Ni sXAS spectra [51]. The intertwined and depth-dependent redox reactions of different TM cations highlight the complexity in the thermally-induced cathode degradation, which is relevant to both the battery performance and safety.

Table 1. Absorption edges of elements for LTMO materials [101].

	K-edge (eV)	L_3-edge (eV)	L_2-edge (eV)
Li	54.7	-	-
Ni	8333	852.7	870
Co	7709	778.1	793.2
Mn	6539	638.7	649.9
O	543.1	18.2	18.2

Although there are a few nice demonstrations in the literature [47, 48], the limited penetration capability of soft X-rays sets practical constrains in the experiment, in particular, for *in-situ*/*operando* type of studies. In this regard, hard X-ray absorption spectroscopy demonstrates considerable advantages. The features in the transition metal *K*-edges' spectra can provide information on the electronic and local lattice structures. It is widely used to probe the chemical valance state of the TM elements in LTMO. Depending on the scanned energy window, hard XAS includes XANES and EXAFS, the former is sensitive to the materials' electronic structures and the latter is often used to probe the lattice structural information and has been discussed in the previous section. Pioneered by Yang *et al., in-situ* XANES has been employed to study the

evolution of the TM elements in LTMO during the cycling process [102]. A comprehensive study of the Ni, Co, and Mn in NMC-333 utilizing *in-situ* XANES was reported by Yoon *et al.* [99], in which the *in-situ* cells were charged up to 5.1 V at a charging rate of 0.05 C while the XANES data over the *K*-edges of Mn, Ni, and Co were collected at set intervals (Fig. 5c). As the Li-ion is deintercalated from the cathode, the Mn XANES spectrum changes its shape without apparent energy shift, while the Ni XANES spectrum shifts toward a higher energy, hinting that the average oxidation state of Ni increases and that of Mn cation is relatively stable during the charging process. The interpretation of the Co K-edge XANES data is a bit more complicated because it is not obvious if the subtle differences in the spectra are caused by the energy shift or by the line-shape deformation [103]. From a more fundamental perspective, the features in the XANES spectra are ultimately associated with the transitions between different electronic states [99]. In the normalized *K*-edge XANES spectra, the weak pre-edge absorption is the electric dipole-forbidden transition of a 1s electron to an unoccupied 3d orbital. The first strong absorption edge features occurring as a shoulder on the lower energy region with respect to the main absorption edge are assigned to a shakedown process involving the 1s → 4p transition followed by ligand-to-metal charge transfer. The main absorption edge features are attributed to the purely dipole-allowed 1s → 4p transition. A more advanced approach for quantifying the XANES data is to conduct a comprehensive and thorough fitting of the entire XANES energy region in terms of well-defined set of structural parameters using a method called MXAN [104]. This method, however, requires a fairly well-defined model and is relatively more time consuming and computationally expensive. Generally, XANES is a powerful method for analyzing the valence state of the TMs in the bulk of the LTMO cathode. The interpretation of XANES data is usually straightforward but might require extra effort when the changes in the spectrum features are subtle.

In all the above discussed spectroscopy techniques, the sample's response to the incident X-rays at a given energy is measured as a scalar. By adding energy resolving power to the detector for an XAS measurement, an additional dimension of the data is extended and more detailed chemical information can be retrieved. Resonant X-ray emission spectroscopy (RXES), often called RIXS, can probe electronic, orbital, magnetic and lattice excitations for the targeted element [48]. The photon-in-photon-out (PIPO) test mode makes RIXS bulk sensitive and its probing depth can reach hundreds of nanometers in soft X-ray regime. The detector's energy resolving power makes it possible to reject unwanted photons and to single out the signal from a specific chemical state. It has been demonstrated that RIXS can distinguish the lattice oxygen redox in LTMO materials, which often overlaps with the transition metal signals and is hard to pick out in a conventional sXAS spectrum. As is shown in Fig. 5d, soft X-ray RIXS over the oxygen *K*-edge was used to probe the evolution of oxygen redox activity in $Li_{1.17}Ni_{0.21}Co_{0.08}Mn_{0.54}O_2$, a model Li-rich layered cathode [100]. In the pristine and 4.35 V-charged electrodes, excitation into the unoccupied TM 3d – O 2p* ($E_{excitation}$, 528-533 eV) and TM 4sp – O 2p* ($E_{excitation}$, $>$533 eV) states results in similar emission energy profiles ($E_{emission}$, 522-527 eV), corresponding to a decay from the delocalized oxygen valance band states to fill the excited O 1s core hole. However, for the 4.6 V-charged electrode, a new emission feature at 523.25 eV emerges. It is clearly distinguished from the TM-O hybridized states and can be attributed to the excitation to the new unoccupied O redox state at 530.8 eV. This feature is considered as a direct evidence of the lattice oxygen redox. Interestingly, this O redox feature reversibly appears even after 500 cycles, suggesting that the anion redox in 3d Li-rich NMC could be active over long-term cycling. Recently, Li *et al.* investigated the oxygen redox behaviors in Li-rich NMC under a mildly elevated temperature (up

to ~100 ℃) [25]. A charge transfer between the bulk oxygen anions and the surface transition metal cations was observed under ~100 ℃. This observation indicates the thermally-driven redistribution of lithium-ions. In addition to the Li-rich NMC cathode, conventional $LiNi_{1/3}Co_{1/3}Mn_{1/3}O_2$ and $LiNiO_2$ are also reported to show the anion redox feature at high potentials [85, 105]. Understanding the anionic redox mechanism can critically inform the designs for next-generation high voltage LTMO cathodes and the RIXS technique has demonstrated unique capability in unraveling the anionic activity with superior sensitivity and accuracy.

4. Synchrotron characterization of LTMO's morphological complexity and evolution

We have elaborated on the multi-scale and high-dimensional morphological complexity in LTMO-based lithium-ion batteries at the beginning of this article (see Fig. 1d). Here we reiterate that such a hierarchical structure entails complicated function and degradation mechanisms that collectively govern the behaviors of the LIB across a broad range of time and length scales. This has motivated many synchrotron-based imaging studies on battery from different perspectives. By virtue of high brightness and low beam emittance, synchrotron X-ray has demonstrated prominent advantages in non-destructive and high-dimensional imaging, which endow the capability of characterizing the LTMO-based LIB with different spatial and temporal resolutions and with structural, compositional, and chemical sensitivities. In this section we discuss a few examples of synchrotron-based imaging study of LIB from the cell scale down to the particle level. These studies target different phenomena that are of both scientific and industrial significance to the battery research and serve as good examples to highlight the effectiveness of synchrotron-based imaging techniques in battery research.

4.1 LTMO LIB's hierarchical structure entails multi-scale degradation mechanisms.

We start this section by discussing a cell-level synchrotron imaging study on LIBs under the thermal runaway conditions, which is a catastrophic effect that lies at the heart of the LIB's safety concerns. As shown in Fig. 6(a-d), synchrotron-based high-frequency tomography and high-framerate radiography were employed to image the dynamic structural evolution of 18650-type commercial cells that were undergoing purposely provoked thermal runaway [106]. By using high-frequency synchrotron tomography, it was observed that the wound electrode layers of the cell with a built-in cylindrical support remained mostly intact before the thermal runaway (Fig. 6a), while noticeable electrode collapse occurred under a similar circumstance in a different cell that has no structural support (Fig. 6b). Although the synchrotron-base micro-tomography can reach to a data rate of ~1 tomogram per second or even slightly higher, it is temporal resolution is still far from sufficient when it comes to capturing the structural dynamics associated with the LIB's thermal runaway. The authors turned to high-speed radiography with a high framerate of 1,250 frames per second (FPS), which largely benefit from the intense X-ray beam generated by a synchrotron facility. Key image frames presented in Fig. 6(c-d) demonstrate interesting morphological features that reveal the internal conditions of this burning LIBs. In the cell with structural support, the copper current collector melted and collected into globules during the thermal runaway, suggesting that the LIB's internal temperature has reached above 1085 ℃, the melting point of copper, while the outer electrode layers remained unbroken, manifesting a huge temperature gradient. This was in part attributed to the ejection of the collapsed spiral-wound materials into the atmosphere, which effectively dissipated the heat. The authors further reported a distinct observation in the cell that has no structural support. Without the structural confinement,

thermal runaway was not observed to propagate throughout the cell. The bulk of the intact contents were ejected soon after the initiation of the thermal runaway. This cell-level battery imaging with high temporal resolution provides a direct and dynamic visualization of the thermal runaway induced structural distortion, breakdown and material ejection, which is otherwise inaccessible. These observations can inform the thermal modelling effort to understand and, potentially, to mitigate the LIB failure with a thermal runaway.

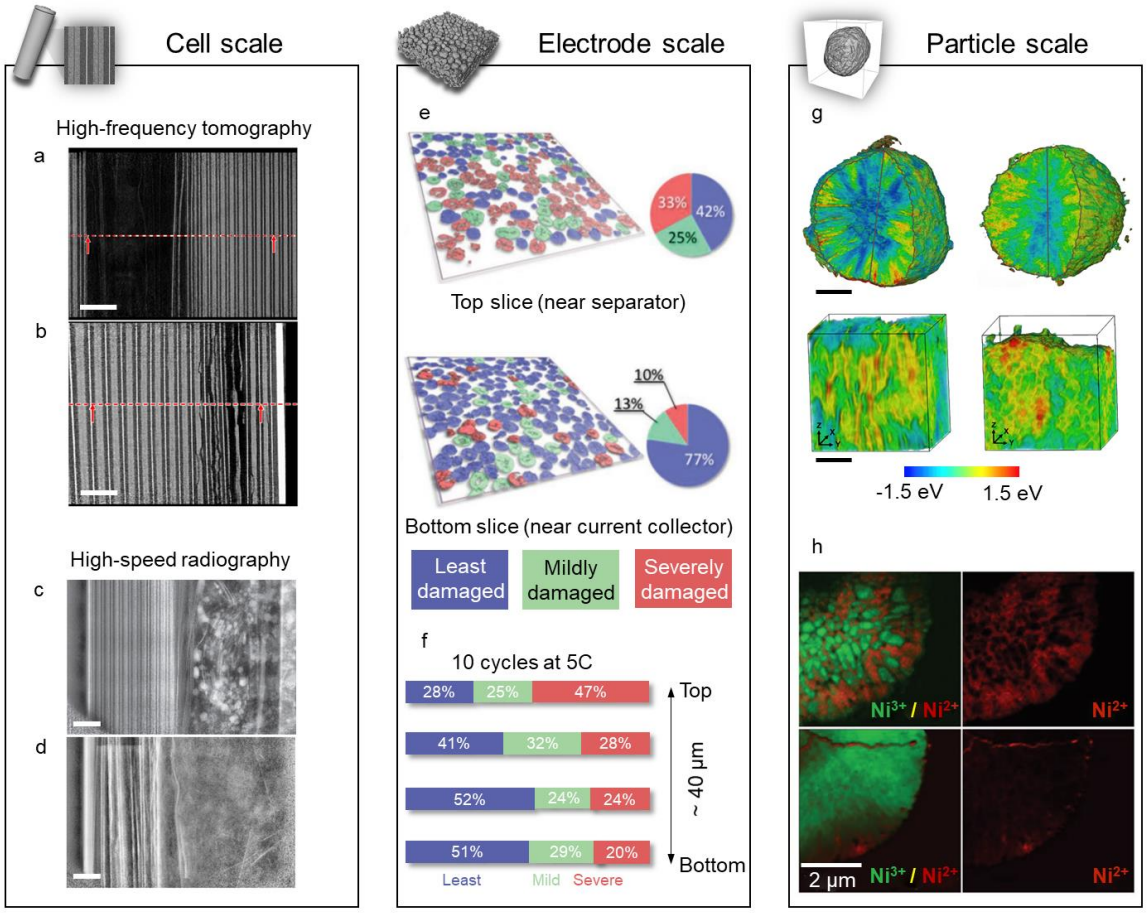

Figure 6. Synchrotron-based X-ray multi-scale imaging studies of LTMO cathode materials. (a-d) Operando high-speed tomography studies of 18650-type cell during thermal runaway, scale bar: 1 mm. Adapted with permission from [106], Copyright 2015, Springer Nature. (e) The degradation comparison of the top and the bottom layers in the $LiNi_{0.2}Mn_{0.2}Co_{0.2}O_2$ electrode. Adapted with permission from [107], Copyright 2019, WILEY - VCH. (f) The fracturing profiles across the top to the bottom of the electrodes after 10 cycles at 5 C rate. Adapted with permission from [107], Copyright 2019, WILEY - VCH. (g) Charge distributions in the first charged rod-NMC (left) and gravel-NMC (right) particles, scale bar: 3 µm. Adapted with permission from [24], Copyright 2020, Springer Nature. (h) Chemical phase maps (red and green represent Ni^{2+} and Ni^{3+}, respectively) of cross sections of conventional (top) and "core-shell" structural (bottom) $LiNi_{0.9}Co_{0.05}Mn_{0.05}O_2$ particles in fully charged after 100 cycles. Adapted with permission from [108], Copyright 2021, WILEY - VCH.

While the above discussed acute LIB failure through thermal runaway accentuates the need for rapid imaging capabilities at a synchrotron beamline, LIBs often experience chronic electrode degradations that feature a multi-scale and complicated electro-chemo-mechanical interplay. The root cause of the LIB degradation over repeated electrochemical cycling lies with the anisotropic lattice expansion and contraction in the active materials, which is accompanied by accumulation of mechanical stress, leading to structural disintegration. For an in-depth investigation of this effect, synchrotron microscopy techniques with high spatial resolution down to nanometer scales become the go-to approach. In particular, the nano-resolution synchrotron X-ray tomography has been demonstrated as a powerful tool for detect the structural damage on the electrode to particle levels nondestructively. As a specific example, here we discuss a study on the nano-resolution imaging of polycrystalline NMC cathode by Yang *et al.* [107]. The polycrystalline NMC composite cathode is vulnerable to the formation of intergranular cracks along the grain boundaries of primary particles, which escalates the electrochemistry decay upon the cycling. While this cracking effect often occurs within individual secondary particles, at the electrode level, the degree of particle fracturing features a highly heterogeneous pattern after fast-charging protocols (as shown in Fig. 6(e-f)). A thorough quantification of these particles in a statistically significant manner is critical to avoiding any pitfall in the interpretation of the experimental results. The authors developed a machine learning method, which they reported in details in a follow-up publication by Jiang *et al.*[109], to conduct the particle identification and quantification automatically. A large number of NMC particles were segmented and labelled based on their respective degrees of fracturing. These results were then quantified for evaluating the depth-dependence in the electrode utilization at different states. In the electrode that was subjected to 10 fast cycles, it was observed that there are more severely damaged particles near the separator than near current collector, which is attributed to a strong cell polarization effect under fast charging conditions. Such a depth-dependent cracking pattern evolved towards a more homogeneous degradation pattern as more particles near the current collector participated in the electrochemical reactions during the later cycles. The authors fed this information into a systematic finite element modeling study and elucidated the underlying mechanism from a theoretical perspective [107]. In addition, thanks to the phase contrast capability in the synchrotron nanoprobe-based nano-tomography approach, noticeable detachment of the NMC particles' from the carbon-binder domain (CBD) was also visualized in the severely damaged local regions [109], which could lead to partial deactivation of NMC particles and to a detriment to the capacity retention.

While acknowledging that these particles are highly heterogenous, meaning that they could respectively exhibit different electrochemical states, they are the architectural building blocks for the electrode and a comprehensive investigation at the particle/sub-particle level can offer valuable insights from the fundamental perspective. At the particle level, the particle morphology has a significantly impact on its electrochemical performance, which, in turn, motivates very active particle engineering efforts in this field. Full-field synchrotron spectro-microscopy and spectro-tomography with ~30 nm spatial resolution has been successfully applied to the study of the battery particles and these efforts were termed the mesoscale battery science. In a recent study by Xu *et al.*, synchrotron spectro-tomography were employed to compare the 3D patterns of redox heterogeneity in NMC cathode particles with different primary grain arrangements (Fig. 6g) [24]. The particle with radially aligned rod grains exhibits a lower electrochemical polarization compared to the counterpart with randomly oriented gravel grains. With the chemical gradient analysis, it was confirmed that the radially aligned rod grains facilitate the Li-ion diffusion in a

rather straight geometrical path with suppressed tortuosity, which, subsequently, improve the charge homogeneity.

As another example for the particle engineering efforts in this field, we refer to the construction of cathode particles with a "Core-Shell" characteristic that is featured by a compositional concentration gradient. This approach was pioneered by Sun *et al.* and they have demonstrated improvements in both specific capacity and cycling stability through this strategy [22]. For example, in the study of $LiNi_{0.9}Co_{0.05}Mn_{0.05}O_2$ doped with 1 mol% Al, the "Core-Shell" structure with aligned grains exhibits a distinct morphology comparing to the conventional structure with randomly oriented grains (Fig. 6h) [108]. The authors employed an energy-resolved transmission soft X-ray microscopy to detect the distribution of Ni valence state over the particle cross-section. Fig. 6h illustrates the morphology and composition modulated Ni valence state distribution over the particles that were harvested after 100 cycles. More Ni^{2+} was detected on the surface of the conventional NCMA particle as evidenced by red borders, suggesting that more severe surface reconstruction took place and produced NiO-like impurities that passivated the primary particles. In contrast, in the particle with core-shell compositional gradient, this damage effect was suppressed and most of the primary particles maintain the Ni^{3+} state.

4.2 LTMO's redox and lattice heterogeneities.

We have already touched upon the redox heterogeneity in LTMO battery cathode in the previous section, here we dive deeper into this topic and will highlight the interplay between the redox and lattice heterogeneities in the later part of this section. While the redox heterogeneity is ubiquitous in LTMO materials and is often regarded as an unwanted phenomenon because it tends to escalate asymmetric stress and cause structure disintegration [110], we would point out that engineering the particle with some degree of redox heterogeneity can potentially improve the cycling stability. For example, the incorporation of Zirconium in to the cathode as a coating layer or a trace dopant could effectively modulate the surface heterogeneity for single-crystal NMC particle and suppress the interfacial lattice reconstruction, benefiting the electrochemical stability at high cut-off voltage [111].

Here, we choose to highlight two studies that elucidate the evolution of the redox heterogeneity in LTMO as a function of the electrochemical states. The first example is a recent study on the depth-dependent redox stratification effect in a Li-rich NMC ($Li_{1.2}Ni_{0.13}Mn_{0.54}Co_{0.13}O_2$) cathode [57]. The complexity in this material lies with the co-existing and intertwined cation and anion redox reactions upon charging to high voltage. The involvement of the lattice oxygen anions in the redox reaction has been reported using advanced synchrotron spectroscopic tools, e.g., soft X-ray resonant inelastic scattering (soft RIXS), which reveals the electronic state of oxygen anion when the cathode is deeply delithiated, as we have elaborated in the previous section of this article, without offering spatial resolution to probe the chemical heterogeneity. In this work by Zhang *et al.*, the authors employed the nano-resolution spectro-tomography method to probe the evolution of the depth-profiles for the oxidations states of all the three transition metal cations in the system (Mn, Co, and Ni). While an anticipated depth-dependent particle polarization effect was observed in the particle that was charged to a low voltage of 4.3 V, surprising nonmonotonic depth profiles were found in material that was charged to 4.8 V (Fig. 7a) with the core and the outermost layer of the fully charged particle showing high Mn valence and the Mn in the transition layers being relatively reduced. Further testing revealed that the valence of Ni gradually increases from particle surface to the core region of the fully charged particle and the Co's valence state has a similar distribution tendency with that of the Mn's valence state. It has been reported that the oxygen

redox reaction in Li-rich LTMO cathode onsets at around 4.4 V. Therefore, the development of the nonmonotonic redox profiles for the transition metal cations was attributed to the involvement of oxygen activity, which also demonstrates a depth-dependent profile that can be inferred indirectly from the behaviors of the transition metal cations. While this example highlights the difference in the spatial profile of the chemical heterogeneity at different electrochemical states for LTMO cathode, an experimental observation of the LTMO particles under *in-situ* conditions would be viewed as a desirable improvement to this study, in particular, for capturing the dynamic evolution over repeated electrochemical cycling. This has motivated a range of synchrotron-based *in-situ* and *operando* imaging studies, including the second example that we will cover next. In a work by Xu *et al.*, a single $LiCoO_2$ particle inside a working pouch cell was monitored as the cell underwent a designed electrochemical cycling process [54]. An unambiguous inverse correlation between cycling C rate and the recovery rate was reported for this particular particle, highlighting the fact that a single cathode particle is able to response differently to different externally applied reaction driving force. In addition to the rate dependence, the rearrangement of the SOC spatial pattern also change under stabilized and repeated cycling conditions (0.2 C, from the 3^{rd} to the 21^{st} cycles). The results indicated, in addition to that the electrochemical redox heterogeneity is highly dependent on the C rate, an electrochemical reactivation process with a small C rate can potentially be designed to recover some of the lost capacity due to the previous fast charging operations. This type of *in-situ* and *operando* synchrotron spectro-imaging measurements has been employed to study the correlation between redox and morphology (size and crystal plane [112]) of the LTMO particles under high C rate. These insights are valuable to the design of high-power-type LTMO materials.

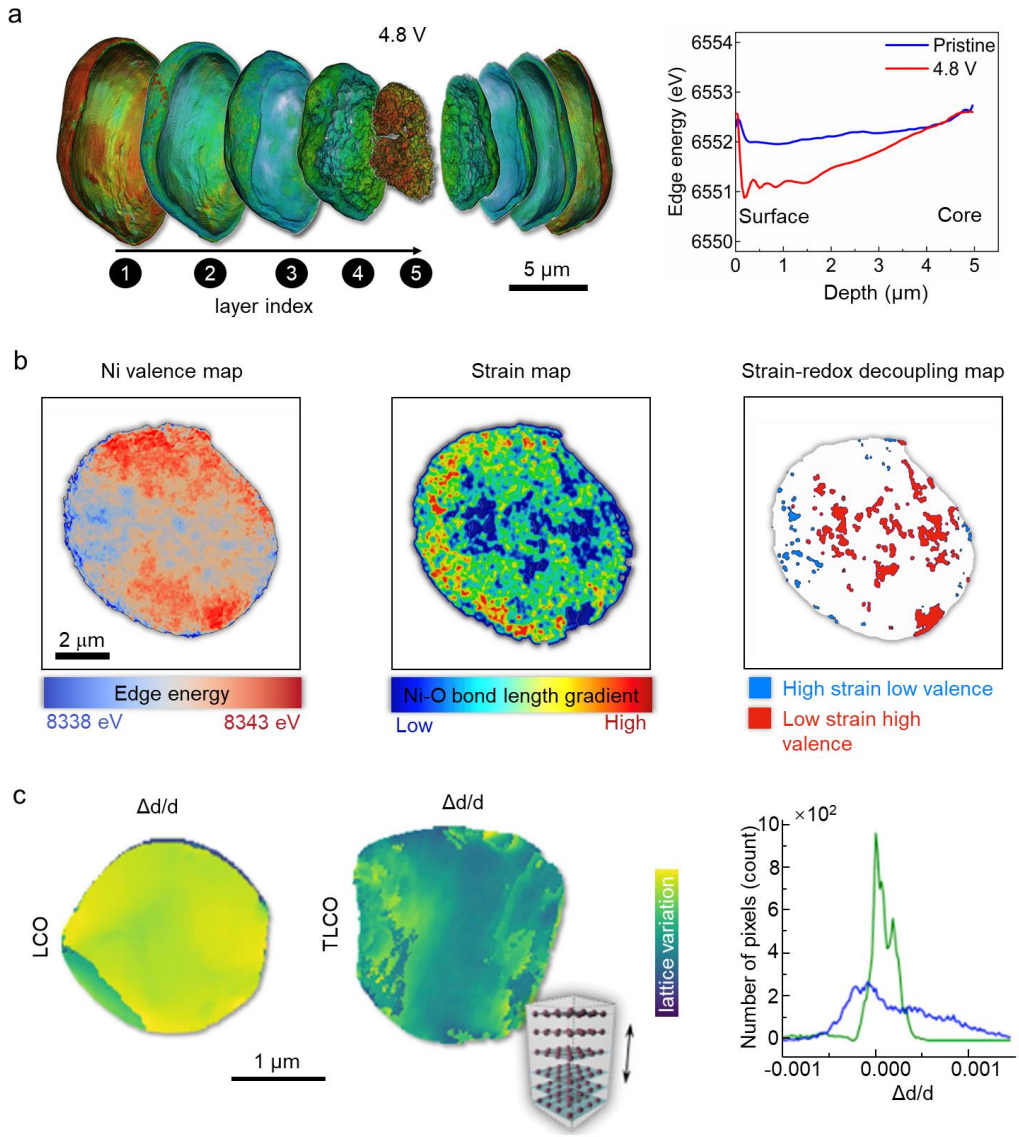

Figure 7. Synchrotron-based X-ray imaging studies of redox and lattice heterogeneities in LTMO cathode materials. (a) The depth-dependent redox stratification effect in a Li-rich NMC ($Li_{1.2}Ni_{0.13}Mn_{0.54}Co_{0.13}O_2$) cathode. Adapted with permission from [57], Copyright 2020, Springer Nature. (b) The inhomogeneous redox and lattice strain in cycled $LiNi_{0.8}Co_{0.1}Mn_{0.1}O_2$ particle. Adapted with permission from [55], Copyright 2021, American Chemical Society. (c) Titanium doping effect on lattice variation in the $LiCoO_2$ particle. Adapted with permission from [90], Copyright 2020, Elsevier.

While the redox heterogeneity is pervasive in LTMO materials, it is often attributed to the morphological complexities, the inhomogeneous distribution of Li ions, and, thus, the local SoC variations. Here we point out that the atomic structural arrangements, including the lattice distortions and defects, have a very significant role to play in affecting the redox heterogeneity and the battery performance. These lattice heterogeneities could be induced by the imperfect

nucleation and crystallization processes during the synthesis, they could also be induced due to undesired side reactions that occur during the battery operation. Synchrotron offers various experimental probes with sensitivity to the material's lattice arrangements, e.g., XRD, EXAFS, and PDF, which we have covered in the previous designated section. Here we discuss the experimental approaches to resolve the lattice heterogeneity in LTMO at the mesoscale with nano-resolution. In a recent development that combines the full-field nano-resolution transmission x-ray microscopy/tomography with the EXAFS scan, Qian *et al.* visualized and correlated the redox features and the lattice bonding features in a cycled poly-crystalline NMC particle (Fig. 7b) [55]. In the presented TXM-EXAFS measurements, the authors extracted the Ni's valence state from the XNAES region and the Ni-O bonding length from the EXAFS region. To address the challenge of low signal-to-noise in the EXAFS spectra, the authors formulated a machine-learning-assisted data clustering approach for reduction of the noise and the dimensionality of the data. Upon recovering a map of the Ni-O bond length over the particle, the authors further quantified the amplitude of the gradient, which is then attributed to a strain induced lattice distortion. While a general position correlation between the redox and the strain was observed, in good agreement with the common wisdom, localized regions with a strain-redox decoupling effect were also observed and attributed to different degradation mechanisms. Combined with 3D nano-tomography, it was found that the regions of high Ni valence and low strain are likely detached from the particle due to cracks and no longer participate the electrochemical reaction. The regions of low Ni valence and high strain, on the other hand, populate on the particle surface and may be the results of surficial lattice reconstruction. This redox-strain coupling/decoupling behavior features the complexity of degradation mechanisms in $LiNi_{0.8}Co_{0.1}Mn_{0.1}O_2$ materials upon prolonged battery operation. This study largely benefits from the correlation analysis of the redox and lattice heterogeneities in LTMO cathode.

Another approach to directly reveal the lattice heterogeneity is to conduct spatially resolved XRD measurement using a small X-ray focal spot. For this purpose, the hard X-ray nanoprobe (HXN) has demonstrated exceptional capability of detecting the lattice structures and their variations in space [90]. In an HXN study of quasi-single-crystalline LTMO material, the X-rays are focused to a spot of ~30 nm onto a sample, producing a spotty diffraction pattern with peaks in the orientations that satisfy the Bragg conditions. The sample can be rocked over a small angular range and a 2D raster scan is often conducted to collect the signals from different parts of the sample. In a recent work by Hong *et al.*, the authors investigated the Titanium dopant's impact on the structure of $LiCoO_2$. They conducted HXN-based mapping to detect the degrees of lattice distortions in Ti-dopped $LiCoO_2$ and in bare $LiCoO_2$ [90]. Their results (Fig. 7c) suggest that the incorporation of a trace amount of Ti into the $LiCoO_2$ lattice has significantly distorted the host lattice due to the incompatibility of the dopant with the $LiCoO_2$ matrix. The heterogeneous lattice configuration increases the energy barrier of anisotropic micro-strain in $LiCoO_2$ particle during delithiation to 4.6 V, suppressing the undesired O3 to H1-3 phase transition, which is evidenced by the improved stability of the Ti-doped $LiCoO_2$ cathode upon high-voltage charging to 4.6 V.

Coherent diffractive X-ray imaging is another method that have demonstrated some success in evaluating the evolution of lattice defects in LTMO upon battery operation. Singer *et al.* studied the nucleation of dislocations defects and their dynamics in lithium-rich LTMO cathode materials during battery charging using Bragg coherent diffractive imaging (BCDI) technique [113]. In their experiment, a rather sophisticated phase retrieval method was used to reconstruct the dislocation networks inside the particle from the Bragg diffraction pattern. As the cathode is charged to a higher voltage, more dislocation defects are formed, which could be associated with the oxygen

evolution. Unfortunately, this effect prevents the authors from evaluating the particle at a voltage above 4.4 V because the phase retrieval method failed at the state with abundant lattice defects. While this is an exciting development with promising future, the technical challenges associated with the coherent X-ray imaging needs to be addressed for practical and routine applications of this method.

5. The correlative synchrotron techniques and scientific data mining.

In the LTMO-based battery material, the electrochemical delithiation/lithiation process is rather intricate, involving morphology and composition effects, electronic and lattice structural evolutions, and sophisticated interplay between the active material and inactive components, e.g., carbon, binder, and electrolyte. An in-depth understanding of this process requires a thorough and systematic investigation into different aspects of the material property. In the previous sections, we have elaborated on the respective strength of various synchrotron-based experimental techniques. Here we highlight that performing these characterizations in a correlative manner can provide unique insights that are otherwise inaccessible. This is particularly the case for the multi-modal imaging of battery materials and we choose to briefly discuss two examples of this kind below.

While it is broadly appreciated that the battery charging/discharging is ultimate a bulk reaction but the surface chemistry has an important role to play in this process, a detailed picture and a fundamental understanding of this surface-to-bulk interaction is rather elusive due to the lack of direct experimental observations. In a work by Li *et al.*, a single poly-crystalline $LiNi_{0.8}Co_{0.1}Mn_{0.1}O_2$ particle were imaged correlatively using both soft and hard X-ray probes with nanoscale spatial resolution (see illustration in Fig. 8) [114]. The hard X-ray nano-tomography reconstructs the 3D internal structure of the particle nondestructively. Meanwhile, the soft X-ray nanoprobe can precisely map out the surface chemical distribution, elucidating the heterogeneous surface reconstruction and passivation effect. By correlating these two measurements, it was observed that the regions with higher porosity in the bulk tend to suffer more severe surface lattice reconstructions. This experimental observation informed a systematic finite element modeling that reveals the coevolution of Li concentration, stress, and the damage function in the NMC secondary particle.

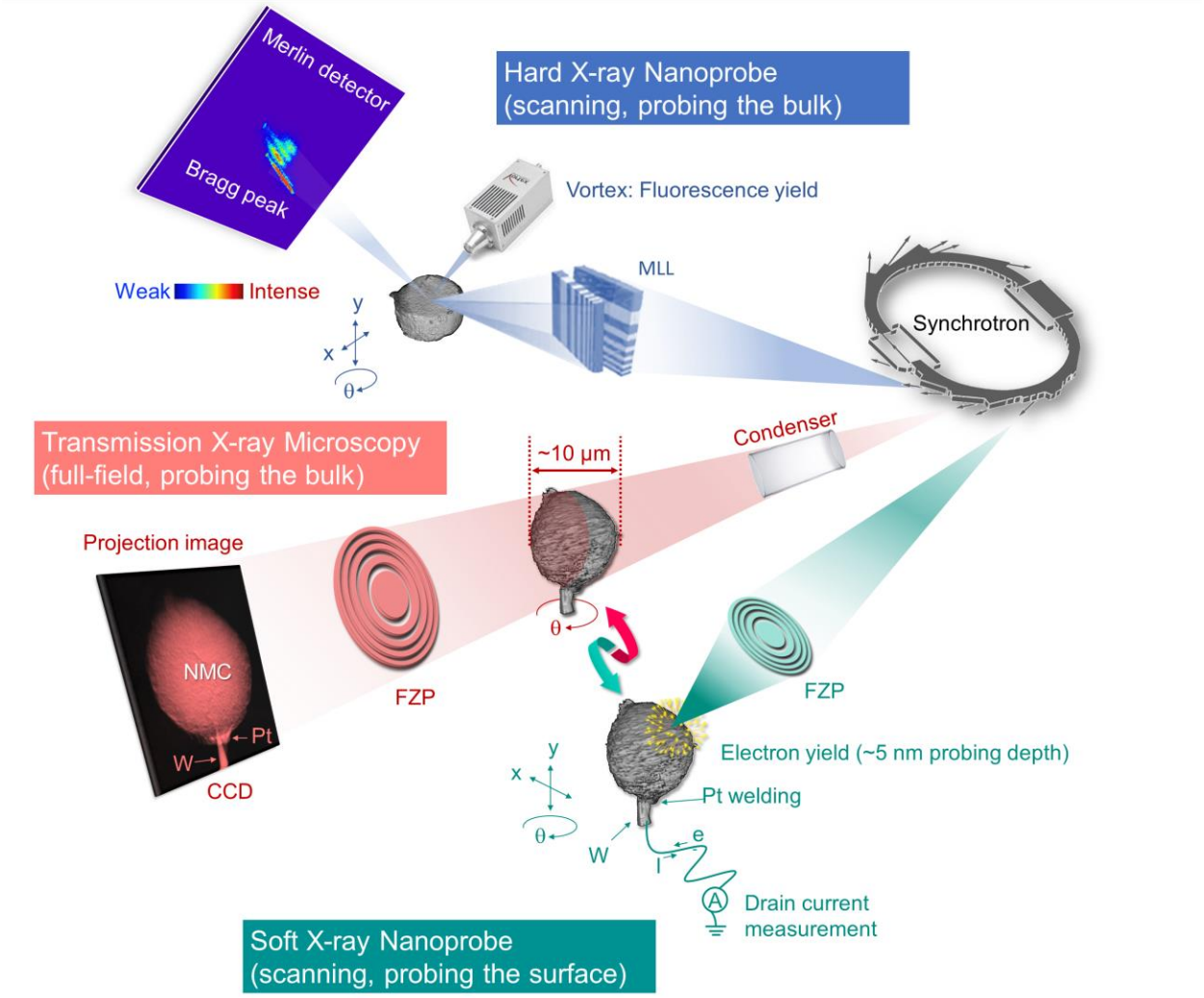

Figure 8. Synchrotron-based correlative analysis of LTMO cathode materials. Adapted with permission from [114], Copyright 2020, Springer Nature. Adapted with permission from [111], Copyright 2021, Elsevier.

Qian *et al.* combined the nano-resolution full-field hard X-ray spectro-tomography and the scanning hard X-ray nanoprobe techniques to investigate a single-crystalline NMC material with a trace amount of Zirconium doping [111]. By correlating the dopant and the SOC distributions at the mesoscale, the authors revealed an interesting pattern of Ni redox inhomogeneity, which suggests that the mesoscale electrochemical kinetic is modulated by the facet-selective Zr segregation. It is useful to highlight that this study leverages the high sensitivity of the scanning nanoprobe and the high efficiency of the full-field spectro-tomography. By putting these two datasets together, it is revealed that the lithium diffusion path parallel to the (003) plane was blocked by a Zr-rich layer segregated on the side edge of the particle, forming kinetically favored particle corners. This result is helpful to understand the dopant's influence and to design novel LTMO materials with engineered compositional arrangements.

Finally, we would like to bring the readers' attention to a new research direction that combines state-of-the-art synchrotron experimental techniques with novel computational developments, e.g., machine learning and data mining, for battery studies. In general, these novel computational methods can greatly assist battery researchers and synchrotron scientists in reducing large scale experimental data and extracting scientifically important information. Machine learning approaches have been utilized to guide high-throughput synchrotron experiments for material screening [115], to conduct classification and dimension reduction for chemical imaging data for capturing undesired side reactions in battery [55, 56, 116], to assist the battery imaging data processing, segmentation, and quantification [57, 107], to construct a numerical model for battery failure and lifetime prediction [117, 118].

For example, to evaluate the chemomechanical breakdown of the LTMO cathode particles, special attention needs to be paid to the statistical analysis in order to avoid any pitfall in the interpretation of the imaging data. This is because the damage pattern is highly heterogeneous and the particles in the same electrode can exhibit a very significant difference in their respective degrees of cracking. As an example, we show in Fig. 9 the synchrotron nano-tomographic results of a NMC composite cathode that is recovered from a fast-cycled coin cell. Within this electrode, the particles exhibit very different cracking pattern as demonstrated by the selected slice-views shown in the bottom row of Fig. 9. Moreover, the particle clusters can also demonstrate different degrees of damaging, indicating their difference in the engagement of the electro-chemo-mechanical processes. The two selected clusters, only ~50 μm apart, are very different in their structural integrity. Machine learning methods can offer much needed assistance in identifying and quantifying the thousands-to-millions of particles in the electrode, with superior accuracy and efficiency. The evaluation of the massive amount of NMC particles (shown in Fig. 9) largely benefits from such a development by Jiang *et al.*, with the source code made openly available to the research community [109].

This is a highly interdisciplinary and rapidly evolving research field. We anticipate to see a very significant growth in the research endeavors in this direction from researchers of different backgrounds.

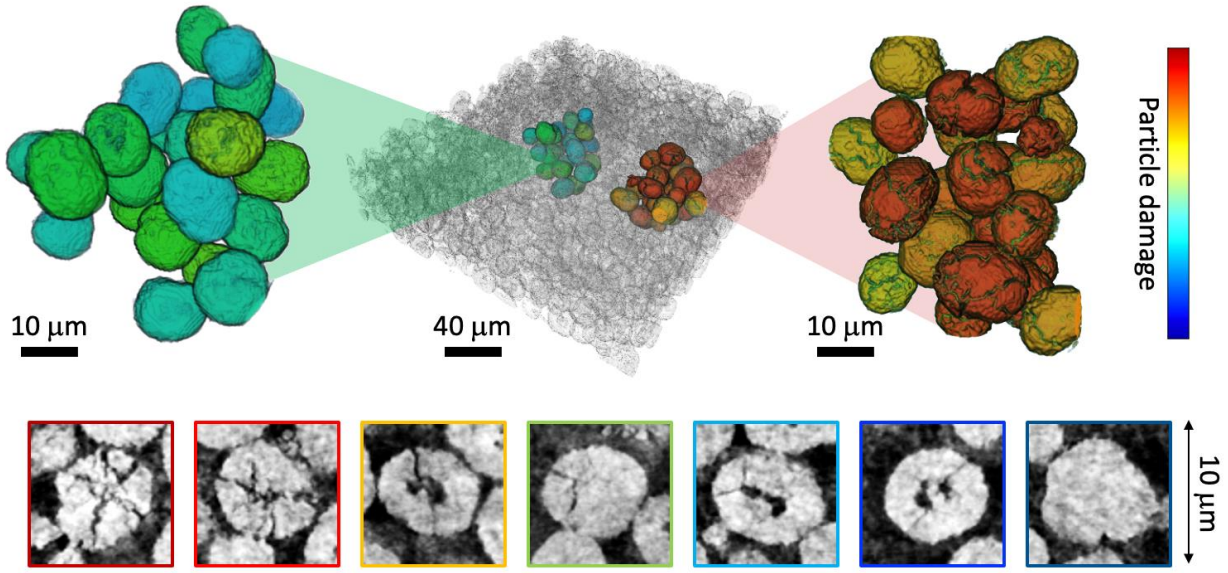

Figure 9. Quantification for NMC particle cracking in real-world composite cathode. These particles exhibit very different cracking pattern (bottom row). The particle clusters also demonstrate different degrees of structural disintegration (top row).

6. Conclusion and Prospective

Rechargeable battery technologies have demonstrated a tremendous impact on the modern society through facilitating the groundbreaking developments in consumer electronics, electric vehicles, and grid energy storage, all of which have demonstrated enormous market value. A practical battery is a highly complicated multi-component device, featuring structural and chemical evolutions at different time and length scales upon battery operation. These battery components work in a synergistic way in order to fulfill the energy storage functionality. There are very active research efforts that look into different battery components, but, at present, the cathode material remains the major bottle neck for improving the energy density. Therefore, we choose LTMO, a leading cathode candidate, as our focus for this review and look into the complicated thermo-electro-chemo-mechanical interplay in LTMO cathode.

For studying such a material system with enormous structural and chemical complexities, advanced characterization tools are indispensable. In particular, the study of practical LTMO cathode with intertwined microstructural, compositional, and chemical heterogeneities needs a holistic suite of experimental methods with different sensitivities. Synchrotron techniques stand out as one of the most effective methods for nondestructive battery characterization with sensitivities to the lattice, electronic, and morphological structures. In this article, we systematically discuss the novel developments in this field. Specifically, we discuss the complexity and evolution of LTMO cathode's structural and chemical properties as the battery is operated under different conditions. We further review relevant synchrotron-based research works that address the frontier challenges in this field and provide novel insights for understanding the battery degradation mechanisms and for informing the effort to improve the battery cathode.

This is a highly active research field. State-of-the-art developments involve efforts from the material science, synchrotron development, and advanced computing. In our review, we included a few recent works that integrate these cutting-edge developments, e.g., *in-situ*/*operando* battery studies at synchrotron, cross-beamline and cross-facility multi-modal synchrotron studies for battery cathode, machine learning and data mining assisted battery studies at synchrotron. These case studies serve as good examples to highlight the interdisciplinary nature of this research field.

Looking forward, we envision that the future research challenges in this field are largely associated with the growing complexity in novel battery materials and systems. In particular, the battery materials' dynamic transformation, involving metastable phases that are functionally critical by are often overlooked in conventional studies, could be important for the novel battery material design. Such a complexity can be further amplified as the batteries are operated under extreme conditions for different applications, e.g., ultra-fast charging, cold/hot climate, and space exploration. The ongoing and projected major upgrades of the synchrotron and free electron lasers (FEL) facilities bring in scientific opportunities for this research field. The enhancements in the X-ray brightness and brilliance could facilitate X-ray experiments with unprecedented resolution and sensitivity, critical to the investigation of next-generation battery materials. The X-ray induced damage effect, however, needs to be carefully considered and addressed to avoid any artifacts associated with the radiation damage. As a concluding remark, we are confident that, with

collaborative efforts from material scientists, synchrotron scientists, and computational scientists, this community is making substantial impacts on the energy storage technology and moving toward a global energy solution with the much desired sustainability.

FUNDING

Stanford Synchrotron Radiation Lightsource is supported by the U.S. Department of Energy (DOE), Office of Science, Office of Basic Energy Sciences under Contract No. DE-AC02-76SF00515. The work at IOP was supported by funding from Natural Science Foundation of Beijing (grant no. Z20J00042) and Newton Advanced Fellowships. This work is also supported by a junior faculty start-up grant of Shanghai Jiao Tong University (to L.S.L.), the Natural Science Foundation of China (22008154 to L.S.L), and partially by Sinopec (420038–1, to L.S.L).

Conflict of interest statement. None declared.

REFERENCES

1. Zeng, X, Li, M, Abd El-Hady, D, *et al.* Commercialization of Lithium Battery Technologies for Electric Vehicles. *Advanced Energy Materials*. 2019; **9**(27): 1900161.
2. Armand, M, Tarascon, JM. Building better batteries. *Nature*. 2008; **451**(7179): 652-7.
3. Li, W, Erickson, EM, Manthiram, A. High-nickel layered oxide cathodes for lithium-based automotive batteries. *Nature Energy*. 2020; **5**(1): 26-34.
4. Fan, E, Li, L, Wang, Z, *et al.* Sustainable Recycling Technology for Li-Ion Batteries and Beyond: Challenges and Future Prospects. *Chemical Reviews*. 2020.
5. Whittingham, MS. Lithium Batteries and Cathode Materials. *Chemical Reviews*. 2004; **104**(10): 4271-302.
6. Manthiram, A, Knight, JC, Myung, S-T, *et al.* Nickel-Rich and Lithium-Rich Layered Oxide Cathodes: Progress and Perspectives. *Advanced Energy Materials*. 2016; **6**(1): 1501010.
7. Ozawa, K. Lithium-ion rechargeable batteries with LiCoO2 and carbon electrodes: the $LiCoO_2$/C system. *Solid State Ionics*. 1994; **69**(3): 212-21.
8. Wang, L, Chen, B, Ma, J, *et al.* Reviving lithium cobalt oxide-based lithium secondary batteries-toward a higher energy density. *Chemical Society Reviews*. 2018; **47**(17): 6505-602.
9. Mizushima, K, Jones, PC, Wiseman, PJ, *et al.* Li_xCoO_2 ($0<x<-1$): A new cathode material for batteries of high energy density. *Materials Research Bulletin*. 1980; **15**(6): 783-9.
10. Ohzuku, T, Makimura, Y. Layered Lithium Insertion Material of $LiCo_{1/3}Ni_{1/3}Mn_{1/3}O_2$ for Lithium-Ion Batteries. *Chemistry Letters*. 2001; **30**(7): 642-3.
11. Liu, W, Oh, P, Liu, X, *et al.* Nickel-Rich Layered Lithium Transition-Metal Oxide for High-Energy Lithium-Ion Batteries. *Angewandte Chemie International Edition*. 2015; **54**(15): 4440-57.
12. Myung, S-T, Maglia, F, Park, K-J, *et al.* Nickel-Rich Layered Cathode Materials for Automotive Lithium-Ion Batteries: Achievements and Perspectives. *ACS Energy Letters*. 2017; **2**(1): 196-223.
13. Xu, J, Lin, F, Doeff, MM, *et al.* A review of Ni-based layered oxides for rechargeable Li-ion batteries. *Journal of Materials Chemistry A*. 2017; **5**(3): 874-901.
14. Van der Ven, A. Lithium Diffusion in Layered Li_xCoO_2. *Electrochemical and Solid-State Letters*. 1999; **3**(7): 301.

15. Kang, K, Ceder, G. Factors that affect Li mobility in layered lithium transition metal oxides. *Physical Review B*. 2006; **74**(9): 094105.
16. Manthiram, A, Vadivel Murugan, A, Sarkar, A, *et al.* Nanostructured electrode materials for electrochemical energy storage and conversion. *Energy & Environmental Science*. 2008; **1**(6): 621-38.
17. Xia, H, Lu, L, Meng, YS, *et al.* Phase Transitions and High-Voltage Electrochemical Behavior of $LiCoO_2$ Thin Films Grown by Pulsed Laser Deposition. *Journal of The Electrochemical Society*. 2007; **154**(4): A337.
18. Li, Y, Xu, Y, Wang, Z, *et al.* Stable Carbon–Selenium Bonds for Enhanced Performance in Tremella-Like 2D Chalcogenide Battery Anode. *Advanced Energy Materials*. 2018; **8**(23): 1800927.
19. Lebens-Higgins, ZW, Sallis, S, Faenza, NV, *et al.* Evolution of the Electrode–Electrolyte Interface of $LiNi_{0.8}Co_{0.15}Al_{0.05}O_2$ Electrodes Due to Electrochemical and Thermal Stress. *Chemistry of Materials*. 2018; **30**(3): 958-69.
20. Sun, HH, Ryu, H-H, Kim, U-H, *et al.* Beyond Doping and Coating: Prospective Strategies for Stable High-Capacity Layered Ni-Rich Cathodes. *ACS Energy Letters*. 2020: 1136-46.
21. Sun, Y-K, Chen, Z, Noh, H-J, *et al.* Nanostructured high-energy cathode materials for advanced lithium batteries. *Nature Materials*. 2012; **11**(11): 942-7.
22. Sun, Y-K, Myung, S-T, Park, B-C, *et al.* High-energy cathode material for long-life and safe lithium batteries. *Nature Materials*. 2009; **8**(4): 320-4.
23. Kim, U-H, Ryu, H-H, Kim, J-H, *et al.* Microstructure-Controlled Ni-Rich Cathode Material by Microscale Compositional Partition for Next-Generation Electric Vehicles. *Advanced Energy Materials*. 2019; **9**(15): 1803902.
24. Xu, Z, Jiang, Z, Kuai, C, *et al.* Charge distribution guided by grain crystallographic orientations in polycrystalline battery materials. *Nature Communications*. 2020; **11**(1): 83.
25. Li, S, Lee, S-J, Wang, X, *et al.* Surface-to-Bulk Redox Coupling through Thermally Driven Li Redistribution in Li- and Mn-Rich Layered Cathode Materials. *Journal of the American Chemical Society*. 2019; **141**(30): 12079-86.
26. Yan, P, Zheng, J, Liu, J, *et al.* Tailoring grain boundary structures and chemistry of Ni-rich layered cathodes for enhanced cycle stability of lithium-ion batteries. *Nature Energy*. 2018; **3**(7): 600-5.
27. Kim, H, Kim, MG, Jeong, HY, *et al.* A New Coating Method for Alleviating Surface Degradation of $LiNi_{0.6}Co_{0.2}Mn_{0.2}O_2$ Cathode Material: Nanoscale Surface Treatment of Primary Particles. *Nano Letters*. 2015; **15**(3): 2111-9.
28. Bi, Y, Tao, J, Wu, Y, *et al.* Reversible planar gliding and microcracking in a single-crystalline Ni-rich cathode. *Science*. 2020; **370**(6522): 1313.
29. Qian, G, Zhang, Y, Li, L, *et al.* Single-crystal nickel-rich layered-oxide battery cathode materials: synthesis, electrochemistry, and intra-granular fracture. *Energy Storage Materials*. 2020; **27**: 140-9.
30. Qian, G, Li, Z, Meng, D, *et al.* Temperature-Swing Synthesis of Large-Size Single-Crystal $LiNi_{0.6}Mn_{0.2}Co_{0.2}O_2$ Cathode Materials. *Journal of the Electrochemical Society*. 2021; **168**(1): 010534.
31. Yang, W. Oxygen release and oxygen redox. *Nature Energy*. 2018; **3**(8): 619-20.
32. Lin, F, Liu, Y, Yu, X, *et al.* Synchrotron X-ray Analytical Techniques for Studying Materials Electrochemistry in Rechargeable Batteries. *Chemical Reviews*. 2017; **117**(21): 13123-86.

33. Balerna, A, Mobilio, S. Introduction to Synchrotron Radiation. In: Mobilio, S, Boscherini, F, Meneghini, C (eds.). *Synchrotron Radiation: Basics, Methods and Applications*. Berlin, Heidelberg: Springer Berlin Heidelberg; 2015. 3-28.
34. Bilderback, DH, Elleaume, P, Weckert, E. Review of third and next generation synchrotron light sources. *Journal of Physics B: Atomic, Molecular and Optical Physics*. 2005; **38**(9): S773-S97.
35. Norman, D. X-ray absorption spectroscopy (EXAFS and XANES) at surfaces. *Journal of Physics C: Solid State Physics*. 1986; **19**(18): 3273-311.
36. de Groot, F. High-Resolution X-ray Emission and X-ray Absorption Spectroscopy. *Chemical Reviews*. 2001; **101**(6): 1779-808.
37. Adams, F, Janssens, K, Snigirev, A. Microscopic X-ray fluorescence analysis and related methods with laboratory and synchrotron radiation sources. *Journal of Analytical Atomic Spectrometry*. 1998; **13**(5): 319-31.
38. Weiland, C, Rumaiz, AK, Pianetta, P, *et al.* Recent applications of hard x-ray photoelectron spectroscopy. *Journal of Vacuum Science & Technology A*. 2016; **34**(3): 030801.
39. Kobayashi, K. Hard X-ray photoemission spectroscopy. *Nuclear Instruments and Methods in Physics Research Section A: Accelerators, Spectrometers, Detectors and Associated Equipment*. 2009; **601**(1): 32-47.
40. Lindau, I, Pianetta, P, Doniach, S, *et al.* X-ray photoemission spectroscopy. *Nature*. 1974; **250**(5463): 214-5.
41. Pérez, CA, Radtke, M, Sánchez, HJ, *et al.* Synchrotron radiation X-Ray fluorescence at the LNLS: beamline instrumentation and experiments. *X-Ray Spectrometry*. 1999; **28**(5): 320-6.
42. Kotani, A, Shin, S. Resonant inelastic x-ray scattering spectra for electrons in solids. *Reviews of Modern Physics*. 2001; **73**(1): 203-46.
43. Ren, Y, Zuo, X. Synchrotron X-Ray and Neutron Diffraction, Total Scattering, and Small-Angle Scattering Techniques for Rechargeable Battery Research. *Small Methods*. 2018; **2**(8): 1800064.
44. Kane, PP. Inelastic scattering of X-rays and gamma rays. *Radiation Physics and Chemistry*. 2006; **75**(12): 2195-205.
45. Caldwell, DO, Eisner, AM, Elings, VB, *et al.* Measurements of Inelastic Compton Scattering. *Physical Review Letters*. 1974; **33**(14): 868-71.
46. Wu, J, Yang, Y, Yang, W. Advances in soft X-ray RIXS for studying redox reaction states in batteries. *Dalton Transactions*. 2020; **49**(39): 13519-27.
47. Li, Q, Qiao, R, Wray, LA, *et al.* Quantitative probe of the transition metal redox in battery electrodes through soft x-ray absorption spectroscopy. *Journal of Physics D: Applied Physics*. 2016; **49**(41): 413003.
48. Yang, W, Devereaux, TP. Anionic and cationic redox and interfaces in batteries: Advances from soft X-ray absorption spectroscopy to resonant inelastic scattering. *Journal of Power Sources*. 2018; **389**: 188-97.
49. Li, W, Li, M, Hu, Y, *et al.* Synchrotron-Based X-ray Absorption Fine Structures, X-ray Diffraction, and X-ray Microscopy Techniques Applied in the Study of Lithium Secondary Batteries. *Small Methods*. 2018; **2**(8): 1700341.
50. Wei, C, Xia, S, Huang, H, *et al.* Mesoscale Battery Science: The Behavior of Electrode Particles Caught on a Multispectral X-ray Camera. *Accounts of Chemical Research*. 2018; **51**(10): 2484-92.
51. Alvarado, J, Wei, C, Nordlund, D, *et al.* Thermal stress-induced charge and structure heterogeneity in emerging cathode materials. *Materials Today*. 2020; **35**: 87-98.
52. Lin, F, Nordlund, D, Li, Y, *et al.* Metal segregation in hierarchically structured cathode materials for high-energy lithium batteries. *Nature Energy*. 2016; **1**(1): 15004.

53. Tian, C, Xu, Y, Nordlund, D, *et al.* Charge Heterogeneity and Surface Chemistry in Polycrystalline Cathode Materials. *Joule*. 2018; **2**(3): 464-77.
54. Xu, Y, Hu, E, Zhang, K, *et al.* In situ Visualization of State-of-Charge Heterogeneity within a $LiCoO_2$ Particle that Evolves upon Cycling at Different Rates. *ACS Energy Letters*. 2017; **2**(5): 1240-5.
55. Qian, G, Zhang, J, Chu, S-Q, *et al.* Understanding the Mesoscale Degradation in Nickel-Rich Cathode Materials through Machine-Learning-Revealed Strain–Redox Decoupling. *ACS Energy Letters*. 2021; **6**(2): 687-93.
56. Mao, Y, Wang, X, Xia, S, *et al.* High-Voltage Charging-Induced Strain, Heterogeneity, and Micro-Cracks in Secondary Particles of a Nickel-Rich Layered Cathode Material. *Advanced Functional Materials*. 2019; **29**(18): 1900247.
57. Zhang, J, Wang, Q, Li, S, *et al.* Depth-dependent valence stratification driven by oxygen redox in lithium-rich layered oxide. *Nature Communications*. 2020; **11**(1): 6342.
58. Delmas, C, Fouassier, C, Hagenmuller, P. Structural classification and properties of the layered oxides. *Physica B & C*. 1980; **99**(1-4): 81-5.
59. Jarvis, KA, Deng, Z, Allard, LF, *et al.* Atomic Structure of a Lithium-Rich Layered Oxide Material for Lithium-Ion Batteries: Evidence of a Solid Solution. *Chemistry of Materials*. 2011; **23**(16): 3614-21.
60. Xu, C, Reeves, PJ, Jacquet, Q, *et al.* Phase Behavior during Electrochemical Cycling of Ni-Rich Cathode Materials for Li-Ion Batteries. *Advanced Energy Materials*. 2021; **11**(7): 2003404.
61. Zeng, X, Li, J, Liu, L. Solving spent lithium-ion battery problems in China: Opportunities and challenges. *Renewable and Sustainable Energy Reviews*. 2015; **52**: 1759-67.
62. Zheng, J, Teng, G, Xin, C, *et al.* Role of Superexchange Interaction on Tuning of Ni/Li Disordering in Layered $Li(Ni_xMn_yCo_z)O_2$. *Journal of Physical Chemistry Letters*. 2017; **8**(22): 5537-42.
63. Li, HH, Yabuuchi, N, Meng, YS, *et al.* Changes in the cation ordering of layered O3 $Li_xNi_{0.5}Mn_{0.5}O_2$ during electrochemical cycling to high voltages: An electron diffraction study. *Chemistry of Materials*. 2007; **19**(10): 2551-65.
64. Jung, S-K, Gwon, H, Hong, J, *et al.* Understanding the Degradation Mechanisms of $LiNi_{0.5}Co_{0.2}Mn_{0.3}O_2$ Cathode Material in Lithium Ion Batteries. *Advanced Energy Materials*. 2014; **4**(1).
65. Wu, Y, Ma, C, Yang, J, *et al.* Probing the initiation of voltage decay in Li-rich layered cathode materials at the atomic scale. *Journal of Materials Chemistry A*. 2015; **3**(10): 5385-91.
66. Eum, D, Kim, B, Kim, SJ, *et al.* Voltage decay and redox asymmetry mitigation by reversible cation migration in lithium-rich layered oxide electrodes. *Nature Materials*. 2020; **19**(4): 419-27.
67. Zheng, J, Xu, P, Gu, M, *et al.* Structural and Chemical Evolution of Li- and Mn-Rich Layered Cathode Material. *Chemistry of Materials*. 2015; **27**(4): 1381-90.
68. Shunmugasundaram, R, Arumugam, RS, Dahn, JR. A Study of Stacking Faults and Superlattice Ordering in Some Li-Rich Layered Transition Metal Oxide Positive Electrode Materials. *Journal of the Electrochemical Society*. 2016; **163**(7): A1394-A400.
69. Breger, J, Jiang, M, Dupre, N, *et al.* High-resolution X-ray diffraction, DIFFaX, NMR and first principles study of disorder in the Li_2MnO_3-$LiNi_{1/2}Mn_{1/2}O_2$ solid solution. *Journal of Solid State Chemistry*. 2005; **178**(9): 2575-85.
70. Meng, YS, Ceder, G, Grey, CP, *et al.* Cation ordering in layered O3 $Li[Ni_xLi_{1/3-2x/3}Mn_{2/3-x/3}]O_2$ ($0<=x<=1/2$) compounds. *Chemistry of Materials*. 2005; **17**(9): 2386-94.
71. Riou, A, Lecerf, A, Gerault, Y, *et al.* Structural study of Li2MnO3. *Materials Research Bulletin*. 1992; **27**(3): 269-75.

72. Croguennec, L, Pouillerie, C, Mansour, AN, *et al.* Structural characterisation of the highly deintercalated $Li_xNi_{1.02}O_2$ phases (with x <= 0.30). *Journal of Materials Chemistry*. 2001; **11**(1): 131-41.
73. Croguennec, L, Pouillerie, C, Delmas, C. NiO_2 obtained by electrochemical lithium deintercalation from lithium nickelate: Structural modifications. *Journal of the Electrochemical Society*. 2000; **147**(4): 1314-21.
74. Li, H, Zhang, N, Li, J, *et al.* Updating the Structure and Electrochemistry of Li_xNiO_2 for 0 <= x <= 1. *Journal of the Electrochemical Society*. 2018; **165**(13): A2985-A93.
75. Croguennec, L, Pouillerie, C, Delmas, C. Structural characterisation of new metastable NiO_2 phases. *Solid State Ionics*. 2000; **135**(1-4): 259-66.
76. Yu, Y-S, Farmand, M, Kim, C, *et al.* Three-dimensional localization of nanoscale battery reactions using soft X-ray tomography. *Nature Communications*. 2018; **9**(1): 921.
77. Zhou, Y-N, Ma, J, Hu, E, *et al.* Tuning charge-discharge induced unit cell breathing in layer-structured cathode materials for lithium-ion batteries. *Nature Communications*. 2014; **5**.
78. Zhou, Y-N, Yue, J-L, Hu, E, *et al.* High-Rate Charging Induced Intermediate Phases and Structural Changes of Layer-Structured Cathode for Lithium-Ion Batteries. *Advanced Energy Materials*. 2016; **6**(21).
79. Breger, J, Dupre, N, Chupas, PJ, *et al.* Short- and long-range order in the positive electrode material, $Li(NiMn)_{(0.5)}O_2$: A joint X-ray and neutron diffraction, pair distribution function analysis and NMR study. *Journal of the American Chemical Society*. 2005; **127**(20): 7529-37.
80. Yu, X, Lyu, Y, Gu, L, *et al.* Understanding the Rate Capability of High-Energy-Density Li-Rich Layered $Li_{1.2}Ni_{0.15}Co_{0.1}Mn_{0.55}O_2$ Cathode Materials. *Advanced Energy Materials*. 2014; **4**(5).
81. Zhu, H, Huang, Y, Ren, J, *et al.* Bridging Structural Inhomogeneity to Functionality: Pair Distribution Function Methods for Functional Materials Development. *Advanced Science*. 2021; **8**(6): 2003534.
82. Kim, MG, Yo, CH. X-ray absorption spectroscopic study of chemically and electrochemically Li ion extracted $Li_yCo_{0.85}Al_{0.15}O_2$ compounds. *Journal of Physical Chemistry B*. 1999; **103**(31): 6457-65.
83. Tsai, YW, Hwang, BJ, Ceder, G, *et al.* In-situ X-ray absorption spectroscopic study on variation of electronic transitions and local structure of $LiNi_{1/3}Co_{1/3}Mn_{1/3}O_2$ cathode material during electrochemical cycling. *Chemistry of Materials*. 2005; **17**(12): 3191-9.
84. Schmidt-Rohr, K. How Batteries Store and Release Energy: Explaining Basic Electrochemistry. *Journal of Chemical Education*. 2018; **95**(10): 1801-10.
85. Lee, G-H, Wu, J, Kim, D, *et al.* Reversible Anionic Redox Activities in Conventional $LiNi_{1/3}Co_{1/3}Mn_{1/3}O_2$ Cathodes. *Angewandte Chemie International Edition*. 2020; **59**(22): 8681-8.
86. Lee, W, Yun, S, Li, H, *et al.* Anionic Redox Chemistry as a Clue for Understanding the Structural Behavior in Layered Cathode Materials. *Small*. 2020; **16**(5): 1905875.
87. Zhao, E, Li, Q, Meng, F, *et al.* Stabilizing the Oxygen Lattice and Reversible Oxygen Redox Chemistry through Structural Dimensionality in Lithium-Rich Cathode Oxides. *Angewandte Chemie International Edition*. 2019; **58**(13): 4323-7.
88. Luo, K, Roberts, MR, Hao, R, *et al.* Charge-compensation in 3d-transition-metal-oxide intercalation cathodes through the generation of localized electron holes on oxygen. *Nature Chemistry*. 2016; **8**(7): 684-91.
89. Liu, L, Li, M, Chu, L, *et al.* Layered ternary metal oxides: Performance degradation mechanisms as cathodes, and design strategies for high-performance batteries. *Progress in Materials Science*. 2020; **111**: 100655.

90. Hong, Y-S, Huang, X, Wei, C, *et al.* Hierarchical Defect Engineering for $LiCoO_2$ through Low-Solubility Trace Element Doping. *Chem*. 2020; **6**(10): 2759-69.
91. Tukamoto, H, West, AR. Electronic Conductivity of $LiCoO_2$ and Its Enhancement by Magnesium Doping. *Journal of The Electrochemical Society*. 1997; **144**(9): 3164-8.
92. Okubo, M, Hosono, E, Kim, J, *et al.* Nanosize Effect on High-Rate Li-Ion Intercalation in $LiCoO_2$ Electrode. *Journal of the American Chemical Society*. 2007; **129**(23): 7444-52.
93. Okubo, M, Kim, J, Kudo, T, *et al.* Anisotropic Surface Effect on Electronic Structures and Electrochemical Properties of $LiCoO_2$. *The Journal of Physical Chemistry C*. 2009; **113**(34): 15337-42.
94. Sun, G, Yu, F-D, Que, L-F, *et al.* Local electronic structure modulation enhances operating voltage in Li-rich cathodes. *Nano Energy*. 2019; **66**: 104102.
95. Foix, D, Sathiya, M, McCalla, E, *et al.* X-ray Photoemission Spectroscopy Study of Cationic and Anionic Redox Processes in High-Capacity Li-Ion Battery Layered-Oxide Electrodes. *The Journal of Physical Chemistry C*. 2016; **120**(2): 862-74.
96. Assat, G, Iadecola, A, Foix, D, *et al.* Direct Quantification of Anionic Redox over Long Cycling of Li-Rich NMC via Hard X-ray Photoemission Spectroscopy. *ACS Energy Letters*. 2018; **3**(11): 2721-8.
97. Assat, G, Foix, D, Delacourt, C, *et al.* Fundamental interplay between anionic/cationic redox governing the kinetics and thermodynamics of lithium-rich cathodes. *Nature Communications*. 2017; **8**(1): 2219.
98. Lin, F, Nordlund, D, Markus, IM, *et al.* Profiling the nanoscale gradient in stoichiometric layered cathode particles for lithium-ion batteries. *Energy & Environmental Science*. 2014; **7**(9): 3077-85.
99. Yoon, W-S, Balasubramanian, M, Chung, KY, *et al.* Investigation of the Charge Compensation Mechanism on the Electrochemically Li-Ion Deintercalated $Li_{1-x}Co_{1/3}Ni_{1/3}Mn_{1/3}O_2$ Electrode System by Combination of Soft and Hard X-ray Absorption Spectroscopy. *Journal of the American Chemical Society*. 2005; **127**(49): 17479-87.
100. Gent, WE, Lim, K, Liang, Y, *et al.* Coupling between oxygen redox and cation migration explains unusual electrochemistry in lithium-rich layered oxides. *Nature Communications*. 2017; **8**(1): 2091.
101. Ravel, B, Newville, M. ATHENA, ARTEMIS, HEPHAESTUS: data analysis for X-ray absorption spectroscopy using IFEFFIT. *Journal of Synchrotron Radiation*. 2005; **12**(4): 537-41.
102. Liu, D, Shadike, Z, Lin, R, *et al.* Review of Recent Development of In Situ/Operando Characterization Techniques for Lithium Battery Research. *Advanced Materials*. 2019; **31**(28): 1806620.
103. Wei, C, Hong, Y, Tian, Y, *et al.* Quantifying redox heterogeneity in single-crystalline $LiCoO_2$ cathode particles. *Journal of Synchrotron Radiation*. 2020; **27**(3): 713-9.
104. Benfatto, M, Della Longa, S, Natoli, CR. The MXAN procedure: a new method for analysing the XANES spectra of metalloproteins to obtain structural quantitative information. *Journal of Synchrotron Radiation*. 2003; **10**(1): 51-7.
105. Li, N, Sallis, S, Papp, JK, *et al.* Unraveling the Cationic and Anionic Redox Reactions in a Conventional Layered Oxide Cathode. *ACS Energy Letters*. 2019; **4**(12): 2836-42.
106. Finegan, DP, Scheel, M, Robinson, JB, *et al.* In-operando high-speed tomography of lithium-ion batteries during thermal runaway. *Nature Communications*. 2015; **6**(1): 6924.
107. Yang, Y, Xu, R, Zhang, K, *et al.* Quantification of Heterogeneous Degradation in Li-Ion Batteries. *Advanced Energy Materials*. 2019; **9**(25): 1900674.

108. Park, N-Y, Ryu, H-H, Park, G-T, *et al.* Optimized Ni-Rich NCMA Cathode for Electric Vehicle Batteries. *Advanced Energy Materials*. 2021; **11**(9): 2003767.
109. Jiang, Z, Li, J, Yang, Y, *et al.* Machine-learning-revealed statistics of the particle-carbon/binder detachment in lithium-ion battery cathodes. *Nature Communications*. 2020; **11**(1): 2310.
110. Xu, Z, Rahman, MM, Mu, L, *et al.* Chemomechanical behaviors of layered cathode materials in alkali metal ion batteries. *Journal of Materials Chemistry A*. 2018; **6**(44): 21859-84.
111. Qian, G, Huang, H, Hou, F, *et al.* Selective dopant segregation modulates mesoscale reaction kinetics in layered transition metal oxide. *Nano Energy*. 2021; **84**: 105926.
112. Hong, L, Li, L, Chen-Wiegart, Y-K, *et al.* Two-dimensional lithium diffusion behavior and probable hybrid phase transformation kinetics in olivine lithium iron phosphate. *Nature Communications*. 2017; **8**(1): 1194.
113. Singer, A, Zhang, M, Hy, S, *et al.* Nucleation of dislocations and their dynamics in layered oxide cathode materials during battery charging. *Nature Energy*. 2018; **3**(8): 641-7.
114. Li, S, Jiang, Z, Han, J, *et al.* Mutual modulation between surface chemistry and bulk microstructure within secondary particles of nickel-rich layered oxides. *Nature Communications*. 2020; **11**(1): 4433.
115. Ren, F, Ward, L, Williams, T, *et al.* Accelerated discovery of metallic glasses through iteration of machine learning and high-throughput experiments. *Science Advances*. 2018; **4**(4): eaaq1566.
116. Zhang, K, Ren, F, Wang, X, *et al.* Finding a Needle in the Haystack: Identification of Functionally Important Minority Phases in an Operating Battery. *Nano Letters*. 2017; **17**(12): 7782-8.
117. Severson, KA, Attia, PM, Jin, N, *et al.* Data-driven prediction of battery cycle life before capacity degradation. *Nature Energy*. 2019; **4**(5): 383-91.
118. Li, W, Zhu, J, Xia, Y, *et al.* Data-Driven Safety Envelope of Lithium-Ion Batteries for Electric Vehicles. *Joule*. 2019; **3**(11): 2703-15.